Received: 1 September 2017 | Revised: 27 November 2018 | Accepted: 4 December 2018

DOI: 10.1002/nla.2231

RESEARCH ARTICLE

WILEY

Direct solution method for the equilibrium problem for elastic stents

Luka Grubišić | Josip Tambača

Department of Mathematics, Faculty of Science, University of Zagreb, Zagreb, Croatia

Correspondence
Luka Grubišić, Department of Mathematics, Faculty of Science, University of Zagreb, Bijenička 30, 10000 Zagreb, Croatia.
Email: luka.grubisic@math.hr

Funding information
Croatian Science Foundation, Grant/Award Number: HRZZ9345

Summary

We are interested in numerical methods for approximating vector-valued functions on a metric graph. As a model problem, we formulate and analyze a numerical method for the solution of the stationary problem for the one-dimensional elastic stent model. The approximation is built using the mixed finite element method. The discretization matrix is a symmetric saddle-point matrix, and we discuss sparse direct methods for the fast and robust solution of the associated equilibrium system. The convergence of the numerical method is proven and the error estimate is obtained. Numerical examples confirm the theoretical estimates.

KEYWORDS

approximation estimates, endovascular stents, finite element method

1 | INTRODUCTION

Endovascular stents are therapeutic devices used to treat narrowing of the blood vessels, the stenosis. They are typically made of stainless steel, so modeling such devices by the theory of linearized elasticity is justified. In a development of new stent designs, a designer searches for a topological configuration that will have improved mechanical properties. This paper provides one simulation method to robustly approximate the solution of the equilibrium problem of a stent.

We consider a stent (Figure 1) to be a linearized elastic body defined as a union of thin struts (see Figure 2) modeled by the one-dimensional model of curved rods from the works of Jurak et al.[1,2] The transmission conditions at joints are given by the continuity of displacement of the middle curve of the strut and infinitesimal rotation of the cross-sections and by the equilibrium of the contact forces and couples. This model has been first formulated in the work of Tambača et al.[3] and then reformulated in the formulation we use in this paper in the work of Čanić et al.[4] Soundness of the model is also confirmed by the convergence result from the work of Griso.[5]

We use the finite element method for the numerical approximation of the solution of the model. The main obstacle in the analysis and numerical approximation of the problem is posed by the inextensibility/unshearability conditions of each strut in the curved rod model. Thus, we use the mixed formulation of the model from the work of Grubišić et al.[6] The unknowns in the mixed formulation are now $\boldsymbol{u}_S$ collecting all displacements of struts and infinitesimal rotations of their cross-sections and $\boldsymbol{p}_S$ collecting all Lagrange multipliers. In the work of Grubišić et al.,[6] the equivalence of the weak and mixed formulation of the continuous model is established using the ellipticity of the energy form and inf sup (Babuska–Brezzi) condition for the form that is used to impose the inextensibility and unshearability (however, in the sequel on both of these conditions, we refer to it as inextensibility).

We then formulate the numerical approximation in the mixed formulation using piecewise polynomial approximation for the unknowns. To be more precise, we use quadratic elements for displacements/rotations (the space is denoted by V_h) and linear (discontinuous) elements for the Lagrange multipliers (the space Q_h). With this choice of elements, the

FIGURE 1 Elastic stent

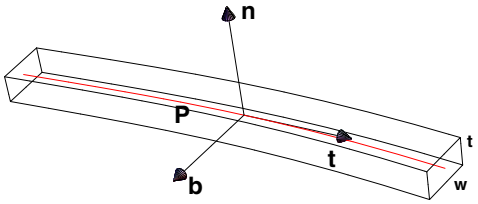

FIGURE 2 3D thin elastic body

energy form k_S is elliptic on the subspace of discretely inextensible displacements V_h^{Ker}. Actually, any choice of elements for the Lagrange multipliers that is larger or equal than the order of elements for displacements/rotations minus one will lead to the ellipticity of the form k_S on V_h^{Ker}. This result then guarantees the existence of solution $\boldsymbol{u}_S$ of the discrete equation (finite-dimensional approximation), but not of the Lagrange multipliers (because we are missing the discrete inf sup inequality). The matrix of the discretized problem will be shown to have the structure of a symmetric saddle-point matrix

$$A = \begin{bmatrix} K & B^* \\ B & 0 \end{bmatrix},$$

where matrix K is a symmetric semidefinite matrix and $\ker(K) \cap \ker(B) = \{0\}$. For a background on saddle-point matrices, see the work of Benzi et al.,[7] and in the context of infinite-dimensional self-adjoint block operator matrices, see the work of Veselić et al.[8] In the terminology of Veselić et al.,[8] symmetric saddle-point matrices whose (1, 1) block is a semidefinite operator are called quasi semidefinite. We have opted to use a more general and more frequent term in this paper and, in general, follow the terminology of Benzi et al.[7] Note that finite elements for elliptic and parabolic problems on metric graphs have been recently studied in the work of Arioli et al.[9]

Matrix A is invertible if and only if in addition $\ker(B^*)$ is trivial. Invertible symmetric saddle-point matrices have a diagonally pivoted block LDL^* factorization $P^*AP = LDL^*$, as described in the work of Duff.[10] The diagonal blocks in D are either 1×1 or 2×2 and L is unit lower triangular. We will see later that matrix L is sparse due to the fact that metric graphs that describe endovascular stents have vertices of the low degree (typically less than four). Alternatively, we will study a perturbed symmetric saddle-point matrix

$$A' = \begin{bmatrix} K & B^* \\ B & -N \end{bmatrix}$$

with N invertible, sparse (diagonal) and $\|N\|$ on the order of the discretization error. The solutions with system matrix A and those with system matrix A' can be related using proposition 4.3.3. of the work of Boffi et al.[11] with the error estimate on the order of $\|N\|$ and so pose a (stabilized) alternative to the use of possibly singular matrix A. For a discussion of the stability of an LDL^* factorization with respect to sparsity controlling pivoting, see the work of Gill et al.[12] For the implementation of the multipliers, we use discontinuous finite elements and so this further reduces fill-ins. Furthermore, we will show that the rank-revealing pivoting strategy (rook-like pivoting) from the works of Fang[13] and Reid et al.[14] is the method that either delivers the unique solution of the discrete problem or detects that $\ker(B^*)$ is nontrivial and so the discrete problem does not have a unique solution.

Even without the discrete inf sup inequality, which would ensure $\ker(B^*)$ were trivial, the error estimate for the displacement/rotation part of the approximation of the solution holds. We use an argument similar to the one used in the works of Boffi et al.[11,15] and build the approximation from V_h, which satisfies the discrete inextensibility condition, that is, it belong to V_h^{Ker}. This then enables us to estimate the error of $\boldsymbol{u}_S - \boldsymbol{u}_S^h$ in the energy norm by the sum of interpolation errors on V_h^{Ker} and Q_h. The interpolation error on V_h^{Ker} that is done strut by strut leaves enough freedom to obtain the h^2 estimates for both interpolations (assuming piecewise quadratic elements). At the end, we also present numerical examples where the mentioned rate of convergence is confirmed.

2 | 1D STENT MODEL

In this section, we shortly describe the stent model for which we build and analyze a numerical approximation. A stent is a 3D elastic body defined as a union of three-dimensional struts. Because the struts are thin comparing to its length, we model their behavior by the 1D curved rod model. The model is given by a system of ODEs defined at the middle curve of the strut, together with the coupling conditions at the points where struts meet, which formulates the 1D elastic stent model. Such 1D stent model was introduced in the work of Tambača et al.[3] and reformulated in the work of Čanić et al.[4] Its justification starting from the 3D equations is achieved in the work of Griso.[5]

2.1 | 1D curved rod model

A three-dimensional elastic body with its two dimensions small comparing to the third is generally called a (curved) elastic rod (see Figure 2). A curved rod model is a one-dimensional approximation whose solution is an approximation of the solution of the equations of the three-dimensional linearized elasticity. The model is given in terms of the arc length of the middle curve of the rod as an unknown variable. Thus, a parametrization $\boldsymbol{P} : [0, l] \to \mathbb{R}^3$ of the middle curve of the curved rod (red in Figure 2) has to be prescribed to formulate the model. Further, let the cross-section of a rod be rectangular of width w in direction of the normal $\boldsymbol{n}$ on the middle curve and thickness t in direction of binormal $\boldsymbol{b}$ on the middle curve.

The one-dimensional equilibrium model for curved elastic rods we use here is given by the following first-order system: find $(\boldsymbol{u}, \boldsymbol{\omega}, \boldsymbol{q}, \boldsymbol{p})$ such that

$$0 = \partial_s \boldsymbol{p} + \boldsymbol{f}, \tag{1}$$

$$0 = \partial_s \boldsymbol{q} + \boldsymbol{t} \times \boldsymbol{p}, \tag{2}$$

$$0 = \partial_s \boldsymbol{\omega} - \mathbf{Q}\mathbf{H}^{-1}\mathbf{Q}^T \boldsymbol{q}, \tag{3}$$

$$0 = \partial_s \boldsymbol{u} + \boldsymbol{t} \times \boldsymbol{\omega}. \tag{4}$$

Here, $\boldsymbol{f}$ is the line density of loads. The first two equations describe the balance of contact force and contact moment, respectively, whereas the last two equations describe the constitutive relation for a curved linearly elastic rod and the condition of inextensibility and unshearability of the rod, respectively. The matrices $\mathbf{H}$ and $\mathbf{Q}$ are given by

$$\mathbf{H} = \begin{bmatrix} EI_{11} & EI_{12} & 0 \\ EI_{12} & EI_{22} & 0 \\ 0 & 0 & \mu K \end{bmatrix}, \qquad \mathbf{Q} = [\, \boldsymbol{t} \;\; \boldsymbol{n} \;\; \boldsymbol{b} \,];$$

see, for example, the work of Cao et al.[16] Here, $E = \mu(3\lambda + 2\mu)/(\lambda + \mu)$ is the Young modulus of the material (μ and λ are the Lamé constants), I_{ij} are the moments of inertia of the cross-sections, and μK is the torsion rigidity of the cross-sections. Therefore, $\mathbf{H}$ describes the elastic properties of the rods (struts) material and the geometry of the cross-sections.

This model is linearization of the Antman–Cosserat model for inextensible, unshearable rods; see the work of Antman[17] or Kosor et al.[18] for the nonlinear rod model and the work of Čanić et al.[4] for the linearization. It was shown in the work of Jurak et al.[2] that the solution of the 1D model can be obtained as a limit of solutions of equilibrium equation of 3D linearized elasticity when the thickness of the cross-sections (w and t) tends to zero. Therefore, for 3D rods that are thin enough, the 1D curved rod model can provide well enough approximation. Moreover, in the work of Tambača,[19] it was shown that curved geometry can be approximated with a piecewise straight geometry with an error estimate for the solution of the associated model. This will further simplify the equations of the 1D model.

2.2 | Differential formulation of the stent model

As mentioned earlier, we model metallic stents as a union of struts modeled by the 1D curved rod model described above. Thus, for defining the 1D stent model, we need to prescribe the following:

- $\mathcal{V}$ set of vertices of the stent (points where middle lines meet);
- $\mathcal{E}$ set of edges of the stent (pairing of vertices), $n_{\mathcal{E}}$ denotes the number of edges;
- $\boldsymbol{P}^i : [0, \ell_i] \to \mathbb{R}^3$ natural parametrization of the middle line of the ith strut (edge $\boldsymbol{e}^i \in \mathcal{E}$);
- μ_i, E_i parameters of material from which the ith strut is made of;
- w^i, t^i width and thickness of the cross-section of the ith strut.

Note that $\mathcal{N} = (\mathcal{V}, \mathcal{E})$ defines a graph and sets the topology of the stent. Adding precise geometry of struts is necessary to define the elastic energy of the stent.

Thus, on the ith strut (edge, $\boldsymbol{e}^i \in \mathcal{E}$), the following system of ODEs holds:

$$0 = \partial_s \boldsymbol{p}^i + \boldsymbol{f}^i, \tag{5}$$

$$0 = \partial_s \boldsymbol{q}^i + \boldsymbol{t}^i \times \boldsymbol{p}^i, \tag{6}$$

$$0 = \partial_s \boldsymbol{\omega}^i - \mathbf{Q}^i(\mathbf{H}^i)^{-1}(\mathbf{Q}^i)^T \boldsymbol{q}^i, \tag{7}$$

$$0 = \partial_s \boldsymbol{u}^i + \boldsymbol{t}^i \times \boldsymbol{\omega}^i. \tag{8}$$

Additionally, we prescribe the coupling conditions at each vertex of the stent net. We assume the following coupling conditions hold:

- the kinematic coupling condition: $(\boldsymbol{u}, \boldsymbol{\omega})$ continuous at each vertex,
- the dynamic coupling condition: balance of contact forces ($\boldsymbol{p}$) and contact moments ($\boldsymbol{q}$) at each vertex.

Thus, Equations (5)–(8) together with these coupling conditions constitute the 1D model of 3D elastic stents. The coupling conditions are justified starting from the three-dimensional nonlinear hyperelasticity in the work of Tambača et al.[20]; see also the work of Griso.[5]

Because the stent is not fixed at any point, we are dealing with a pure traction problem. Therefore, as usual, the solution is not unique and there is an associated necessary condition for the existence. It is easy to check that the functions

$$\boldsymbol{u}^i(s) = \text{const}_y - \boldsymbol{P}^i(s) \times \text{const}_\theta, \qquad \boldsymbol{\omega}^i(s) = \text{const}_\theta, \qquad i = 1, \ldots, n_\mathcal{E} \tag{9}$$

satisfy (5)–(8) for zero loads ($\boldsymbol{f}^i = 0, i = 1, \ldots, n_\mathcal{E}$). Accompanied with this nonuniqueness are necessary conditions for the existence

$$\sum_{i=1}^{n_\mathcal{E}} \int_0^{\ell_i} \boldsymbol{f}^i(s) ds = 0, \qquad \sum_{i=1}^{n_\mathcal{E}} \int_0^{\ell_i} \boldsymbol{P}^i(s) \times \boldsymbol{f}^i(s) ds = 0. \tag{10}$$

These conditions are exactly equilibrium conditions for forces and moments. For more details, see the work of Tambača et al.[21] The associated function space for the force density is therefore

$$L^2_{\text{eq}} = \left\{ \boldsymbol{f} \in L^2(\mathcal{N}; \mathbb{R}^3) \,:\, (10) \quad \text{holds} \right\}.$$

2.3 | Mixed formulation of the stent model

In order to build the numerical approximation, we rewrite the model in the mixed formulation to simplify the construction of finite elements. As usual the kinematic coupling conditions are included into the space of test functions, thereby requiring that the solution must satisfy the continuity of displacement and the continuity of infinitesimal rotation at every net vertex. Due to the trace theorem on Sobolev spaces, these conditions will be imposed in the definition of the space of H^1-functions $\boldsymbol{u}$, defined on the entire stent net $\mathcal{E}$. The vector function $\boldsymbol{u}_S$ consists of all the state variables $(\boldsymbol{u}, \boldsymbol{\omega})$ defined on all the edges $\boldsymbol{e}^i, i = 1, \ldots, n_\mathcal{E}$ so that

$$\boldsymbol{u} = \left((\boldsymbol{u}^1, \boldsymbol{\omega}^1), \ldots, (\boldsymbol{u}^{n_\mathcal{E}}, \boldsymbol{\omega}^{n_\mathcal{E}}) \right).$$

The kinematic coupling condition requires that the displacement of the middle line $\boldsymbol{u}$ and the infinitesimal rotation of the cross-section $\boldsymbol{\omega}$ are continuous at every vertex $\boldsymbol{V} \in \mathcal{V}$. We place the continuity in the function space and thus, for $k \in \mathbb{N}$, define the space

$$H^1(\mathcal{N}; \mathbb{R}^k) = \left\{ \boldsymbol{u} \in \prod_{i=1}^{n_\mathcal{E}} H^1(0, \ell_i; \mathbb{R}^k) \,:\, \boldsymbol{u}^i((\boldsymbol{P}^i)^{-1}(\boldsymbol{V})) = \boldsymbol{u}^j((\boldsymbol{P}^j)^{-1}(\boldsymbol{V})), \right.$$
$$\left. \boldsymbol{\omega}^i((\boldsymbol{P}^i)^{-1}(\boldsymbol{V})) = \boldsymbol{\omega}^j((\boldsymbol{P}^j)^{-1}(\boldsymbol{V})), \quad \forall \boldsymbol{V} \in \mathcal{V}, \boldsymbol{V} \in \boldsymbol{e}^i \cap \boldsymbol{e}^j \right\}.$$

The associated norm is given by

$$\|\boldsymbol{u}_S\|_{H^1(\mathcal{N}; \mathbb{R}^k)} = \left(\sum_{i=1}^{n_\mathcal{E}} \|\boldsymbol{u}^i\|^2_{H^1(0, \ell_i; \mathbb{R}^k)} + \|\boldsymbol{\omega}^i\|^2_{H^1(0, \ell_i; \mathbb{R}^k)} \right)^{1/2}.$$

The dynamic coupling conditions, however, are imposed in the weak sense in the weak/mixed formulation of the underlying equations.

Further, to obtain the problem with a unique solution, we search for the solution with zero-mean displacement and infinitesimal rotation

$$\sum_{i=1}^{n_\varepsilon}\int_0^{\ell_i}\boldsymbol{u}^i ds=\sum_{i=1}^{n_\varepsilon}\int_0^{\ell_i}\boldsymbol{\omega}^i ds=0.$$

To get to the weak formulation of the mixed formulation of the stent problem, we sum up the weak forms of the mixed formulations for each strut for test functions defined on the whole stent, that is, $H^1(\mathcal{N};\mathbb{R}^6)$. Then, by the dynamic contact conditions, contact couples and forces at the strut ends from the equations for all edges cancel out; see the work of Grubišić et al.[6] for more details.

Let the relevant function spaces be denoted by

$$V_S=H^1(\mathcal{N};\mathbb{R}^6),\qquad Q_S=L^2(\mathcal{N};\mathbb{R}^3)\times\mathbb{R}^3\times\mathbb{R}^3=\prod_{i=1}^{n_\varepsilon}L^2(0,\ell_i;\mathbb{R}^3)\times\mathbb{R}^3\times\mathbb{R}^3$$

and let us define bilinear forms obtained by summing the associated forms for each rod as

$$\begin{aligned}
&k_S:V_S\times V_S\to\mathbb{R},\qquad k_S(\boldsymbol{u}_S,\tilde{\boldsymbol{u}}_S)=\sum_{i=1}^{n_\varepsilon}\int_0^{\ell_i}\mathbf{Q}^i\mathbf{H}^i(\mathbf{Q}^i)^T\partial_s\boldsymbol{\omega}^i\cdot\partial_s\tilde{\boldsymbol{\omega}}^i ds,\\
&b_S:Q_S\times V_S\to\mathbb{R},\qquad b_S(\boldsymbol{p}_S,\tilde{\boldsymbol{u}}_S)=\sum_{i=1}^{n_\varepsilon}\int_0^{\ell_i}\boldsymbol{p}^i\cdot(\partial_s\tilde{\boldsymbol{u}}^i+\boldsymbol{t}^i\times\tilde{\boldsymbol{\omega}}^i)ds+\boldsymbol{\alpha}\cdot\sum_{i=1}^{n_\varepsilon}\int_0^{\ell_i}\tilde{\boldsymbol{u}}^i ds+\boldsymbol{\beta}\cdot\sum_{i=1}^{n_\varepsilon}\int_0^{\ell_i}\tilde{\boldsymbol{\omega}}^i ds
\end{aligned}\tag{11}$$

and the linear functional as

$$l_S:V_S\to\mathbb{R},\qquad l_S(\tilde{\boldsymbol{u}}_S)=\sum_{i=1}^{n_\varepsilon}\int_0^{\ell_i}\boldsymbol{f}^i\cdot\tilde{\boldsymbol{u}}^i ds.$$

Here, the used notation is

$$\boldsymbol{p}_S=(\boldsymbol{p}^1,\ \dots,\boldsymbol{p}^{n_\varepsilon},\boldsymbol{\alpha},\boldsymbol{\beta}),$$

whereas the natural norm for Q_S is defined by

$$\|\boldsymbol{p}_S\|=\left(\sum_{i=1}^{n_\varepsilon}\|\boldsymbol{p}^i\|^2_{L^2(0,\ell_i;\mathbb{R}^3)}+\|\boldsymbol{\alpha}\|^2+\|\boldsymbol{\beta}\|^2\right)^{1/2}.$$

Now, the mixed formulation of the stent problem (5)–(8) is given by the following. Find $(\boldsymbol{u}_S,\boldsymbol{p}_S)\in V_S\times Q_S$ such that

$$\begin{aligned}
&k_S(\boldsymbol{u}_S,\tilde{\boldsymbol{u}}_S)+b_S(\boldsymbol{p}_S,\tilde{\boldsymbol{u}}_S)=l_S(\tilde{\boldsymbol{u}}_S),\quad \tilde{\boldsymbol{u}}_S\in V_S,\\
&b_S(\tilde{\boldsymbol{p}}_S,\boldsymbol{u}_S)=0.\qquad \tilde{\boldsymbol{p}}_S\in Q_S,
\end{aligned}\tag{12}$$

However, the weak formulation is given by the following. find $\boldsymbol{u}_S\in V_S^{\mathrm{Ker}}$ such that

$$k_S(\boldsymbol{u}_S,\tilde{\boldsymbol{u}}_S)=l_S(\tilde{\boldsymbol{u}}_S),\quad \tilde{\boldsymbol{u}}_S\in V_S^{\mathrm{Ker}},\tag{13}$$

where

$$\begin{aligned}
V_S^{\mathrm{Ker}}&=\left\{\tilde{\boldsymbol{u}}_S\in V_S:\partial_s\tilde{\boldsymbol{u}}^i+\boldsymbol{t}^i\times\tilde{\boldsymbol{\omega}}^i=0, i=1,\ \dots,n_\varepsilon,\sum_{i=1}^{n_\varepsilon}\tilde{\boldsymbol{u}}^i=\sum_{i=1}^{n_\varepsilon}\tilde{\boldsymbol{\omega}}^i=0\right\}\\
&=\left\{\tilde{\boldsymbol{u}}_S\in V_S:b_S(\tilde{\boldsymbol{p}}_S,\tilde{\boldsymbol{u}}_S)=0,\quad \tilde{\boldsymbol{p}}_S\in Q_S\right\}.
\end{aligned}$$

More details on the model can be found in the work of Čanić et al.[4] The model is not limited for stents; it can be used to model any elastic structure made of rods. It is rigorously justified in the work of Griso[5] starting from the three-dimensional linearized elasticity.

The mixed formulation turns out especially important in problems with constraints that are difficult to satisfy by the finite elements. It is easy to check that any solution $(\boldsymbol{u}_S,\boldsymbol{p}_S)\in V_S\times Q_S$ of the mixed formulation (12) is a solution of the weak formulation (12). The opposite relays on the inf-sup inequality.

From the mixed formulation, it is also easy to conclude the regularity result, namely, for $\boldsymbol{f} \in L^2(\mathcal{N};\mathbb{R}^3)$, one has

$$\boldsymbol{p}^i \in H^1(0,\ell_i), \quad \boldsymbol{q}^i \in H^2(0,\ell_i), \quad \boldsymbol{\omega}^i \in H^3(0,\ell_i), \quad \boldsymbol{u}^i \in H^4(0,\ell_i).$$

Even more smoothness is obtained if the force density is assumed more regular on edges, for example, if it belongs to one of spaces

$$L^2_{H^k}(\mathcal{N};\mathbb{R}^k) = \left\{\boldsymbol{g} \in L^2(\mathcal{N};\mathbb{R}^k) \,:\, \boldsymbol{g}|_{\boldsymbol{e}^i} \in H^k(0,\ell_i;\mathbb{R}^k)\right\}.$$

Further, the strong formulation is then given by the following. Find $(\boldsymbol{u}^i,\boldsymbol{\omega}^i,\boldsymbol{q}^i,\boldsymbol{p}^i)$, $i=1,\ \ldots,n_{\mathcal{E}}$ and $\boldsymbol{\alpha},\boldsymbol{\beta}\in\mathbb{R}^3$ that satisfy the equations at edges

$$\begin{aligned}
&\partial_s \boldsymbol{p}^i - \boldsymbol{\alpha} + \boldsymbol{f}^i = 0, \qquad i=1,\ \ldots,n_{\mathcal{E}},\\
&\partial_s \boldsymbol{q}^i + \boldsymbol{t}^i \times \boldsymbol{p}^i - \boldsymbol{\beta} = 0, \qquad i=1,\ \ldots,n_{\mathcal{E}},\\
&\partial_s \boldsymbol{\omega}^i - \mathbf{Q}^i(\mathbf{H}^i)^{-1}(\mathbf{Q}^i)^T\boldsymbol{q}^i = 0, \qquad i=1,\ \ldots,n_{\mathcal{E}},\\
&\partial_s \boldsymbol{u}^i + \boldsymbol{t}^i \times \boldsymbol{\omega}^i = 0, \qquad i=1,\ \ldots,n_{\mathcal{E}},
\end{aligned} \tag{14}$$

zero-mean displacement and rotation conditions

$$\sum_{i=1}^{n_{\mathcal{E}}} \int_0^{\ell_i} \boldsymbol{u}^i ds = \sum_{i=1}^{n_{\mathcal{E}}} \int_0^{\ell_i} \boldsymbol{\omega}^i ds = 0 \tag{15}$$

and the kinematic and dynamic contact conditions at vertices as follows:

$$\begin{aligned}
&\sum_{i\in J_j^+} \boldsymbol{p}^i(\ell^i) - \sum_{i\in J_j^-} \boldsymbol{p}^i(0) = 0, \qquad j=1,\ \ldots,n_{\mathcal{V}},\\
&\sum_{i\in J_j^+} \boldsymbol{q}^i(\ell^i) - \sum_{i\in J_j^-} \boldsymbol{q}^i(0) = 0, \qquad j=1,\ \ldots,n_{\mathcal{V}},\\
&\boldsymbol{\Theta}^j = \boldsymbol{\omega}^i(0) = \boldsymbol{\omega}^k(\ell^k), \qquad i\in J_j^-, k\in J_j^+, \qquad j=1,\ \ldots,n_{\mathcal{V}},\\
&\boldsymbol{Y}^j = \boldsymbol{u}^i(0) = \boldsymbol{u}^k(\ell^k), \qquad i\in J_j^-, k\in J_j^+, \qquad j=1,\ \ldots,n_{\mathcal{V}};
\end{aligned} \tag{16}$$

here, J_j^- stands for the set of all edges that leave (i.e., the local variable is equal 0 at) the vertex j and J_j^+ stands for the set of all edges that enter (i.e., the local variable is equal ℓ at) the vertex j. Furthermore,

$$\begin{aligned}
\boldsymbol{\alpha} &= \sum_{i=1}^{n_{\mathcal{E}}} \int_0^{\ell_i} \boldsymbol{f}^i ds \Big/ \sum_{i=1}^{n_{\mathcal{E}}} \ell_i,\\
\boldsymbol{\beta} &= \left(\sum_{i=1}^{n_{\mathcal{E}}} \int_0^{\ell_i} \boldsymbol{f}^i \times \boldsymbol{P}^i(s) ds + \boldsymbol{\alpha} \times \sum_{i=1}^{n_{\mathcal{E}}} \int_0^{\ell_i} \boldsymbol{P}^i(s) ds\right) \Big/ \sum_{i=1}^{n_{\mathcal{E}}} \ell_i.
\end{aligned}$$

These follow after inserting the displacements and infinitesimal rotations from the kernel, that is, of the form (9), in the mixed formulation (12).

Note that the weak formulation of the stent problem (13) will have a unique solution as a consequence of Proposition 1 because the form k_S is $\mathbb{K}$–elliptic. In addition, there is no necessary condition for the existence. The role here has been done by the multipliers $\boldsymbol{\alpha}$ and $\boldsymbol{\beta}$ because they are chosen such that $\boldsymbol{fl}-\boldsymbol{\alpha}$ satisfies the necessary conditions of the form (10).

Note further that if we start initially with loads that satisfy (9), then $\boldsymbol{\alpha}=\boldsymbol{\beta}=0$. We fix this in the rest of this paper.

Next, we state results proven in the work of Grubišić et al.[6]

Definition 1. The stent belongs to the class S if one of the following is satisfied.

- all edges are curved;
- there are straight edges. Then,

$$\sum_{i\in J_j^+} \alpha_i \boldsymbol{t}^i - \sum_{i\in J_j^-} \alpha_i \boldsymbol{t}^i = 0, \quad j=1,\ \ldots,n_{\mathcal{V}}, \quad \Leftrightarrow \quad \alpha_i = 0, \quad i=1,\ \ldots,n_{\mathcal{N}};$$

here, $\alpha_i = 0$ for edges that are not straight.

Proposition 1.

(1) The form k_S is V_S^{Ker}–elliptic.
(2) Let the stent be in the class $\mathcal{S}$. Then, there is $\beta_{BB} > 0$ such that

$$\inf_{\tilde{\boldsymbol{p}}_S \in Q_S} \sup_{\tilde{\boldsymbol{u}}_S \in V_S} \frac{b_S(\tilde{\boldsymbol{p}}_S, \tilde{\boldsymbol{u}}_S)}{\|\tilde{\boldsymbol{p}}_S\|_{Q_S} \|\tilde{\boldsymbol{u}}_S\|_{V_S}} \geq \beta_{BB}.$$

(3) For every $l_S \in L^2(0, \ell; \mathbb{R}^3)'$, the problem (12) has a unique solution $(\boldsymbol{u}_S, \boldsymbol{p}_S)$. This solution satisfies also the problem (13).
(4) The problem (13) has a unique solution $\boldsymbol{u}_S \in V_S^{\mathrm{Ker}}$. Then, there is $\boldsymbol{p}_S \in Q_S$ such that $(\boldsymbol{u}_S, \boldsymbol{p}_S)$ satisfies (12).
(5) There exists a constant C such that

$$\|\boldsymbol{u}_S\|_{V_S} + \|\boldsymbol{p}_S\|_{Q_S} \leq C_{LBB} \|l_S\|_{L^2(0,\ell;\mathbb{R}^3)}.$$

Proof. The existence of solutions of (13) is a direct consequence of (1), continuity of forms k_S and b_S and linear functional l_S, and the Lax–Milgram lemma. Remaining statements are consequences of (2) and classical results about the linear variational problems with constraints; see theorem 4.1 and corollary 4.1 of the work of Girault et al.[22] or theorem 4.2.4 of the work of Boffi et al.[11] □

3 | PIECEWISE POLYNOMIAL DISCRETIZATION

We discretize this problem using one-dimensional finite element approximation of (12). We proceed only for stent geometries given by the straight rods. This will ensure that the polynomial approximation we use in finite elements can satisfy the inextensibility condition.

3.1 | Formulation of the method

As the first step, we divide each edge (strut) of the stent into smaller pieces to obtain finer mesh. In this way, we keep the structure unchanged but change its description (number of vertices, number of edges, we split parametrizations, etc.). However, the problem remains given by the equations of the same form (12) on the associated function space. Let us assume that, after these divisions, we obtain stent with $n_{\mathcal{E}}$ edges and $n_{\mathcal{V}}$ vertices.

On edge $\boldsymbol{e}^i$, the projection of the solution $(\boldsymbol{u}_S|_{\boldsymbol{e}^i}, \boldsymbol{p}_S|_{\boldsymbol{e}^i})$ belongs to $H^1(0, \ell^i; \mathbb{R}^6) \times L^2(0, \ell^i; \mathbb{R}^3)$. For the finite-dimensional approximation $(\boldsymbol{u}_S^h|_{\boldsymbol{e}^i}, \boldsymbol{p}_S^h|_{\boldsymbol{e}^i})$, we assume that it belongs to $P^m(\boldsymbol{e}^i; \mathbb{R}^6) \times P^n(\boldsymbol{e}^i; \mathbb{R}^3)$, for some $m, n \in \mathbb{N}$; here, $P^k(\boldsymbol{e}^i; \mathbb{R}^j)$ denotes the space of functions with values in $\mathbb{R}^j$ with all components that are polynomials with degree less or equal k. Thus, the finite-dimensional approximation of the overall stent model will be given on the space $V_h \times Q_h$ with

$$V_h = \left\{ \boldsymbol{u}_S \in H^1(\mathcal{N}; \mathbb{R}^6) \,:\, \boldsymbol{u}_S|_{\boldsymbol{e}^i} \in P^m(\boldsymbol{e}^i; \mathbb{R}^6), i = 1, \ldots, n_{\mathcal{E}} \right\},$$
$$Q_h = \left\{ \boldsymbol{p}_S \in L^2(\mathcal{N}; \mathbb{R}^3) \,:\, \boldsymbol{p}_S|_{\boldsymbol{e}^i} \in P^n(\boldsymbol{e}^i; \mathbb{R}^3), i = 1, \ldots, n_{\mathcal{E}} \right\}.$$

Note that, because V_h is a subset of $H^1(\mathcal{N}; \mathbb{R}^6)$, the functions from V_h are globally continuous on the stent and the finite element approximation is conforming.

The discrete problem that we now consider is given by the following. Find $(\boldsymbol{u}_S^h, \boldsymbol{p}_S^h) \in V_h \times Q_h$ such that

$$\begin{aligned} &k_S\left(\boldsymbol{u}_S^h, \tilde{\boldsymbol{u}}_S\right) + b_S\left(\boldsymbol{p}_S^h, \tilde{\boldsymbol{u}}_S\right) = l_S(\tilde{\boldsymbol{u}}_S), \quad \tilde{\boldsymbol{u}}_S \in V_h, \\ &b_S\left(\tilde{\boldsymbol{p}}_S, \boldsymbol{u}_S^h\right) = 0, \qquad \tilde{\boldsymbol{p}}_S \in Q_h. \end{aligned} \tag{17}$$

To obtain the existence of the weak formulation of the problem (13), one needs ellipticity of k_S on V_S^{Ker}. A discrete variant of the ellipticity will allow to obtain existence and uniqueness of $\boldsymbol{u}_S^h$ in the discrete variant of V_S^{Ker}, which is denoted by

$$V_h^{\mathrm{Ker}} = \left\{ \tilde{\boldsymbol{u}}_S \in V_h \,:\, b_S(\tilde{\boldsymbol{p}}_S, \tilde{\boldsymbol{u}}_S) = 0, \quad \tilde{\boldsymbol{p}}_S \in Q_h \right\}.$$

Namely, if $(\boldsymbol{u}_S^h, \boldsymbol{p}_S^h) \in V_h \times Q_h$ is the solution of (17), then $\boldsymbol{u}_S^h$ satisfies

$$k_S\left(\boldsymbol{u}_S^h, \tilde{\boldsymbol{u}}_S\right) = l_S(\tilde{\boldsymbol{u}}_S), \quad \tilde{\boldsymbol{u}}_S \in V_h^{\mathrm{Ker}}.$$

For V_h^{Ker}-elliptic form k_S, such $\boldsymbol{u}_S^h$ exists by Lax–Milgram. The V_h^{Ker} ellipticity of k_S will also allow to obtain the error estimates for the numerical approximation.

3.2 | Discrete ellipticity of k_S

Lemma 1. *Let $n \geq m - 1$. The form k_S is then V_h^{Ker} elliptic.*

Proof. The space V_h is finite dimensional. Therefore, it is somewhat easier to show ellipticity of the form. Namely, it is enough to show that

$$k_S(\tilde{\boldsymbol{u}}_S, \tilde{\boldsymbol{u}}_S) > 0, \qquad 0 \neq \tilde{\boldsymbol{u}}_S \in V_h^{\mathrm{Ker}}.$$

It is obvious from the definition of k_S that $k_S \geq 0$. k_S is equal to zero

$$k_S(\tilde{\boldsymbol{u}}_S, \tilde{\boldsymbol{u}}_S) = \sum_{i=1}^{n_{\mathcal{E}}} \int_0^{\ell_i} \mathbf{Q}^i \mathbf{H}^i (\mathbf{Q}^i)^T \partial_s \tilde{\boldsymbol{\omega}}^i \cdot \partial_s \tilde{\boldsymbol{\omega}}^i ds = 0$$

if and only if

$$\partial_s \tilde{\boldsymbol{\omega}}^i = 0, \qquad i = 1, \ldots, \mathcal{E}.$$

This implies that $\tilde{\boldsymbol{\omega}}^i$ are constants, and due to continuity of functions from V_h, all constants have to be equal. Because of the condition from V_h^{Ker} that

$$\sum_{i=1}^{n_{\mathcal{E}}} \int_0^{\ell_i} \tilde{\boldsymbol{\omega}}^i ds = 0,$$

we obtain that

$$\tilde{\boldsymbol{\omega}}^i = 0, \qquad i = 1, \ldots, n_{\mathcal{E}}.$$

Now, the condition in V_h^{Ker} implies

$$0 = b_S(\tilde{\boldsymbol{p}}_S, \tilde{\boldsymbol{u}}_S) = \sum_{i=1}^{n_{\mathcal{E}}} \int_0^{\ell_i} \tilde{\boldsymbol{p}}^i \cdot \partial_s \tilde{\boldsymbol{u}}^i ds + \tilde{\boldsymbol{\alpha}} \cdot \sum_{i=1}^{n_{\mathcal{E}}} \int_0^{\ell_i} \tilde{\boldsymbol{u}}^i ds, \qquad \tilde{\boldsymbol{p}}_S \in Q_h.$$

Because all $\tilde{\boldsymbol{p}}^i$, $i = 1, \ldots, n_{\mathcal{E}}$ and $\tilde{\boldsymbol{\alpha}}$ are chosen independently, this implies

$$0 = \int_0^{\ell_i} \tilde{\boldsymbol{p}}^i \cdot \partial_s \tilde{\boldsymbol{u}}^i ds, \quad \tilde{\boldsymbol{p}}^i \in P^2, \qquad \sum_{i=1}^{n_{\mathcal{E}}} \int_0^{\ell_i} \tilde{\boldsymbol{u}}^i ds = 0. \tag{18}$$

Because $\partial_s \tilde{\boldsymbol{u}}^i \in P^{m-1}$ and $\tilde{\boldsymbol{p}}^i$ are arbitrary in P^n, we obtain that $\partial_s \tilde{\boldsymbol{u}}^i = 0$. Together with continuity of $\tilde{\boldsymbol{u}}_S$ on the stent structure, this implies that all $\tilde{\boldsymbol{u}}^i$ are equal to the same constant, and because of the second condition from (18), this constant is zero. Thus, the kernel of k_S in V_h^{Ker} is trivial, and thus, it is V_h^{Ker} elliptic. □

Remark 1. One can show, by dimension counting, that in the case $n < m - 1$, the discrete ellipticity does not hold.

3.3 | Interpolation estimates for the solution $(\boldsymbol{u}_S, \boldsymbol{p}_S)$

As usual, error estimates for the finite element method are based on the interpolation estimates for the solution of the problem. Therefore, in this subsection, we approximate an arbitrary solution of the stent problem $(\boldsymbol{u}_S, \boldsymbol{p}_S)$ by piecewise polynomials and derive the estimates. To be more precise, we use the piecewise quadratic polynomials for $\boldsymbol{u}_S$ and piecewise linear polynomials for $\boldsymbol{p}_S$, that is, in the sequel, we fix $m = 2$ and $n = 1$ in the definition of V_h and Q_h.

Because $\boldsymbol{u}_S$ is a solution of the stent problem (12) for $\boldsymbol{f} \in L^2_{\mathrm{eq}}$, we have that $\boldsymbol{u}_S \in V_S^{\mathrm{Ker}}$. Moreover, by the regularity theory, we have that $\boldsymbol{\omega}^i \in H^3(0, \ell_i; \mathbb{R}^3)$ and $\boldsymbol{u}^i \in H^4(0, \ell_i; \mathbb{R}^3)$. Estimates we do edge by edge by fixing first the values of the element from V_S^{Ker} on the given edge $\boldsymbol{e}$ (with generic length ℓ):

$$(\boldsymbol{u}, \boldsymbol{\omega}) = \boldsymbol{u}_S|_{\boldsymbol{e}}.$$

These functions satisfy the inextensibility conditions on edges

$$\boldsymbol{u}'(s) + \boldsymbol{t} \times \boldsymbol{\omega}(s) = 0, \qquad s \in (0, \ell) \tag{19}$$

because $\boldsymbol{u}_S \in V_S^{\mathrm{Ker}}$; here, $\boldsymbol{t}$ is the constant tangent vector of edge $\boldsymbol{e}$. We also fix the values of functions $\boldsymbol{u}, \boldsymbol{\omega}$ at the endpoints of the edge

$$\boldsymbol{Y}_0 = \boldsymbol{u}(0), \quad \boldsymbol{Y}_\ell = \boldsymbol{u}(\ell), \quad \boldsymbol{\Theta}_0 = \boldsymbol{\omega}(0), \quad \boldsymbol{\Theta}_\ell = \boldsymbol{\omega}(\ell)$$

to be able obtain overall solution that belongs to $H^1(\mathcal{N}; \mathbb{R}^6)$.

We build the approximation made of quadratic polynomials

$$\boldsymbol{u}^a(s) = \boldsymbol{a}s^2 + \boldsymbol{b}s + \boldsymbol{c}, \qquad \boldsymbol{\omega}^a(s) = \boldsymbol{d}s^2 + \boldsymbol{e}s + \boldsymbol{g}$$

such that they coincide with $(\boldsymbol{u}, \boldsymbol{\omega})$ for $s \in \{0, \ell\}$, that is,

$$\boldsymbol{u}^a(0) = \boldsymbol{Y}_0, \quad \boldsymbol{u}^a(\ell) = \boldsymbol{Y}_\ell, \quad \boldsymbol{\omega}^a(0) = \boldsymbol{\Theta}_0, \quad \boldsymbol{\omega}^a(\ell) = \boldsymbol{\Theta}_\ell \tag{20}$$

and such that they satisfy the approximate discrete inextensibility condition

$$0 = \int_0^\ell \tilde{\boldsymbol{p}} \cdot \left((\boldsymbol{u}^a)'(s) + \boldsymbol{t} \times \boldsymbol{\omega}^a(s) \right) ds = \int_0^\ell \tilde{\boldsymbol{p}} \cdot \left(2\boldsymbol{a}s + \boldsymbol{b} + \boldsymbol{t} \times (\boldsymbol{d}s^2 + \boldsymbol{e}s + \boldsymbol{f}) \right) ds, \quad \tilde{\boldsymbol{p}} \in P^1. \tag{21}$$

From the boundary condition at $s = 0$ from (20), we obtain $\boldsymbol{c} = \boldsymbol{Y}_0, \boldsymbol{f} = \boldsymbol{\Theta}_0$, whereas from the boundary condition at $s = \ell$ from (20), we now obtain

$$\boldsymbol{Y}_\ell = \boldsymbol{a}\ell^2 + \boldsymbol{b}\ell + \boldsymbol{Y}_0, \qquad \boldsymbol{\Theta}_\ell = \boldsymbol{d}\ell^2 + \boldsymbol{e}\ell + \boldsymbol{\Theta}_0,$$

which imply

$$\boldsymbol{b} = \frac{\boldsymbol{Y}_\ell - \boldsymbol{Y}_0}{\ell} - \boldsymbol{a}\ell, \qquad \boldsymbol{e} = \frac{\boldsymbol{\Theta}_\ell - \boldsymbol{\Theta}_0}{\ell} - \boldsymbol{d}\ell. \tag{22}$$

Now, the discrete inextensibility from (21) implies

$$0 = 2\boldsymbol{a}\frac{\ell^2}{2} + \boldsymbol{b}\ell + \boldsymbol{t} \times \left(\boldsymbol{d}\frac{\ell^3}{3} + \boldsymbol{e}\frac{\ell^2}{2} + \boldsymbol{\Theta}_0\ell \right),$$
$$0 = 2\boldsymbol{a}\frac{\ell^3}{3} + \boldsymbol{b}\frac{\ell^2}{2} + \boldsymbol{t} \times \left(\boldsymbol{d}\frac{\ell^4}{4} + \boldsymbol{e}\frac{\ell^3}{3} + \boldsymbol{\Theta}_0\frac{\ell^2}{2} \right).$$

Inserting (22), we obtain

$$0 = 2\boldsymbol{a}\frac{\ell^2}{2} + \left(\frac{\boldsymbol{Y}_\ell - \boldsymbol{Y}_0}{\ell} - \boldsymbol{a}\ell \right)\ell + \boldsymbol{t} \times \left(\boldsymbol{d}\frac{\ell^3}{3} + \left(\frac{\boldsymbol{\Theta}_\ell - \boldsymbol{\Theta}_0}{\ell} - \boldsymbol{d}\ell \right)\frac{\ell^2}{2} + \boldsymbol{\Theta}_0\ell \right),$$
$$0 = 2\boldsymbol{a}\frac{\ell^3}{3} + \left(\frac{\boldsymbol{Y}_\ell - \boldsymbol{Y}_0}{\ell} - \boldsymbol{a}\ell \right)\frac{\ell^2}{2} + \boldsymbol{t} \times \left(\boldsymbol{d}\frac{\ell^4}{4} + \left(\frac{\boldsymbol{\Theta}_\ell - \boldsymbol{\Theta}_0}{\ell} - \boldsymbol{d}\ell \right)\frac{\ell^3}{3} + \boldsymbol{\Theta}_0\frac{\ell^2}{2} \right).$$

After simplification, the equations for $\boldsymbol{a}$ and $\boldsymbol{d}$ are

$$0 = \boldsymbol{Y}_\ell - \boldsymbol{Y}_0 + \boldsymbol{t} \times \left(-\frac{\ell^3}{6}\boldsymbol{d} + \frac{\ell}{2}(\boldsymbol{\Theta}_\ell - \boldsymbol{\Theta}_0) + \boldsymbol{\Theta}_0\ell \right),$$
$$0 = \frac{\ell^3}{6}\boldsymbol{a} + \frac{\ell}{2}(\boldsymbol{Y}_\ell - \boldsymbol{Y}_0) + \boldsymbol{t} \times \left(-\frac{\ell^4}{12}\boldsymbol{d} + \frac{\ell^2}{3}(\boldsymbol{\Theta}_\ell - \boldsymbol{\Theta}_0) + \boldsymbol{\Theta}_0\frac{\ell^2}{2} \right),$$

that is,

$$0 = \boldsymbol{Y}_\ell - \boldsymbol{Y}_0 + \boldsymbol{t} \times \left(-\frac{\ell^3}{6}\boldsymbol{d} + \frac{\ell}{2}(\boldsymbol{\Theta}_\ell + \boldsymbol{\Theta}_0) \right),$$
$$0 = \frac{\ell^3}{6}\boldsymbol{a} + \frac{\ell}{2}(\boldsymbol{Y}_\ell - \boldsymbol{Y}_0) + \boldsymbol{t} \times \left(-\frac{\ell^4}{12}\boldsymbol{d} + \frac{\ell^2}{3}\boldsymbol{\Theta}_\ell + \frac{\ell^2}{6}\boldsymbol{\Theta}_0 \right).$$

The first equation is solved for $\boldsymbol{d}$, and then, the second gives the solution for $\boldsymbol{a}$. The necessary condition for the existence of solutions of the first equation

$$\boldsymbol{t} \cdot (\boldsymbol{Y}_\ell - \boldsymbol{Y}_0) = 0$$

is fulfilled because (19) holds! The solution is given by

$$\boldsymbol{d} = -\frac{6}{\ell^3}\boldsymbol{t} \times (\boldsymbol{Y}_\ell - \boldsymbol{Y}_0) + \frac{3}{\ell^2}(\boldsymbol{\Theta}_\ell + \boldsymbol{\Theta}_0) + \varphi\boldsymbol{t}, \tag{23}$$

for arbitrary $\varphi \in \mathbb{R}$ because $\boldsymbol{t}\times(\boldsymbol{t}\times\boldsymbol{j}) = \boldsymbol{t}(\boldsymbol{j}\cdot\boldsymbol{t}) - \boldsymbol{j}$. Then,

$$\begin{aligned}
\boldsymbol{a} &= -\frac{3}{\ell^2}(\boldsymbol{Y}_\ell - \boldsymbol{Y}_0) - \boldsymbol{t}\times\left(-\frac{\ell}{2}\left(-\frac{6}{\ell^3}\boldsymbol{t}\times(\boldsymbol{Y}_\ell - \boldsymbol{Y}_0) + \frac{3}{\ell^2}(\boldsymbol{\Theta}_\ell + \boldsymbol{\Theta}_0) + \varphi\boldsymbol{t}\right) + \frac{2}{\ell}\boldsymbol{\Theta}_\ell + \frac{1}{\ell}\boldsymbol{\Theta}_0\right)\\
&= -\frac{3}{\ell^2}(\boldsymbol{Y}_\ell - \boldsymbol{Y}_0) - \boldsymbol{t}\times\left(\frac{3}{\ell^2}\boldsymbol{t}\times(\boldsymbol{Y}_\ell - \boldsymbol{Y}_0) - \frac{3}{2\ell}\boldsymbol{\Theta}_\ell - \frac{3}{2\ell}\boldsymbol{\Theta}_0 + \frac{2}{\ell}\boldsymbol{\Theta}_\ell + \frac{1}{\ell}\boldsymbol{\Theta}_0\right)\\
&= -\frac{3}{\ell^2}(\boldsymbol{Y}_\ell - \boldsymbol{Y}_0) - \boldsymbol{t}\times\left(\frac{3}{\ell^2}\boldsymbol{t}\times(\boldsymbol{Y}_\ell - \boldsymbol{Y}_0) + \frac{1}{2\ell}\boldsymbol{\Theta}_\ell - \frac{1}{2\ell}\boldsymbol{\Theta}_0\right)\\
&= -\frac{3}{\ell^2}(\boldsymbol{Y}_\ell - \boldsymbol{Y}_0) - \frac{3}{\ell^2}\boldsymbol{t}\times(\boldsymbol{t}\times(\boldsymbol{Y}_\ell - \boldsymbol{Y}_0)) - \frac{1}{2\ell}\boldsymbol{t}\times(\boldsymbol{\Theta}_\ell - \boldsymbol{\Theta}_0)\\
&= -\frac{3}{\ell^2}(\boldsymbol{Y}_\ell - \boldsymbol{Y}_0) + \frac{3}{\ell^2}(\boldsymbol{Y}_\ell - \boldsymbol{Y}_0) - \frac{1}{2\ell}\boldsymbol{t}\times(\boldsymbol{\Theta}_\ell - \boldsymbol{\Theta}_0)\\
&= -\frac{1}{2\ell}\boldsymbol{t}\times(\boldsymbol{\Theta}_\ell - \boldsymbol{\Theta}_0).
\end{aligned} \tag{24}$$

Therefore, we have determined all the coefficients of $\boldsymbol{u}^a$ and $\boldsymbol{\omega}^a$ uniquely up to the constant φ. We fix φ in order to obtain the best error estimates. To simplify the computation, we fix them now and just check the estimates

$$\varphi = -\frac{6}{\ell^3}\left(\boldsymbol{\Theta}_0\ell + \boldsymbol{\omega}'(0)\frac{\ell^2}{2} + \boldsymbol{\omega}''(0)\frac{\ell^3}{6}\right)\cdot\boldsymbol{t}. \tag{25}$$

Next, we estimate the H^1 error in approximation of $\boldsymbol{u}$ and $\boldsymbol{\omega}$ by $\boldsymbol{u}^a$ and $\boldsymbol{\omega}^a$ for the obtained coefficients. In order to do that, we use the Taylor theorem for functions in Sobolev spaces. The error estimate is obtained simply from the integral form of the remainder. Namely, we use the following expansion: There is $C > 0$ such that

$$\boldsymbol{\omega}(s) = \boldsymbol{\Theta}_0 + \boldsymbol{\omega}'(0)s + \frac{1}{2}\boldsymbol{\omega}''(0)s^2 + \boldsymbol{R}_\theta(s), \qquad |\boldsymbol{R}_\theta(s)| \le Cs^{5/2}\|\boldsymbol{\omega}'''\|_{L^2(0,\ell;\mathbb{R}^3)}. \tag{26}$$

For the expansion of $\boldsymbol{u}'$, we use the inextensibility condition (19) and (26):

$$\begin{aligned}
\boldsymbol{Y}_\ell - \boldsymbol{Y}_0 &= \int_0^\ell \boldsymbol{u}'(s)ds = -\boldsymbol{t}\times\int_0^\ell \boldsymbol{\omega}(s)ds = -\boldsymbol{t}\times\int_0^\ell\left(\boldsymbol{\Theta}_0 + \boldsymbol{\omega}'(0)s + \frac{1}{2}\boldsymbol{\omega}''(0)s^2 + \boldsymbol{R}_\theta(s)\right)ds\\
&= -\boldsymbol{t}\times\left(\boldsymbol{\Theta}_0\ell + \boldsymbol{\omega}'(0)\frac{\ell^2}{2} + \boldsymbol{\omega}''(0)\frac{\ell^3}{6} + \int_0^\ell \boldsymbol{R}_\theta(s)ds\right).
\end{aligned}$$

Using these expansions in $\boldsymbol{d}$ and $\boldsymbol{e}$ gives (here, we again use $\boldsymbol{t}\times(\boldsymbol{t}\times\boldsymbol{j}) = \boldsymbol{t}(\boldsymbol{j}\cdot\boldsymbol{t}) - \boldsymbol{j}$)

$$\begin{aligned}
\boldsymbol{d} &= \frac{6}{\ell^3}\boldsymbol{t}\times\left(\boldsymbol{t}\times\left(\boldsymbol{\Theta}_0\ell + \boldsymbol{\omega}'(0)\frac{\ell^2}{2} + \boldsymbol{\omega}''(0)\frac{\ell^3}{6} + \int_0^\ell \boldsymbol{R}_\theta(s)ds\right)\right)\\
&\quad + \frac{3}{\ell^2}\left(\boldsymbol{\Theta}_0 + \boldsymbol{\omega}'(0)\ell + \frac{1}{2}\boldsymbol{\omega}''(0)\ell^2 + \boldsymbol{R}_\theta(\ell) + \boldsymbol{\Theta}_0\right) + \varphi\boldsymbol{t}\\
&= \frac{6}{\ell^3}\boldsymbol{t}\left(\boldsymbol{\Theta}_0\ell + \boldsymbol{\omega}'(0)\frac{\ell^2}{2} + \boldsymbol{\omega}''(0)\frac{\ell^3}{6} + \int_0^\ell \boldsymbol{R}_\theta(s)ds\right)\cdot\boldsymbol{t}\\
&\quad - \frac{6}{\ell^3}\left(\boldsymbol{\Theta}_0\ell + \boldsymbol{\omega}'(0)\frac{\ell^2}{2} + \boldsymbol{\omega}''(0)\frac{\ell^3}{6} + \int_0^\ell \boldsymbol{R}_\theta(s)ds\right)\\
&\quad + \frac{3}{\ell^2}\left(2\boldsymbol{\Theta}_0 + \boldsymbol{\omega}'(0)\ell + \frac{1}{2}\boldsymbol{\omega}''(0)\ell^2 + \boldsymbol{R}_\theta(\ell)\right) + \varphi\boldsymbol{t}\\
&= \frac{1}{2}\boldsymbol{\omega}''(0) - \frac{6}{\ell^3}\int_0^\ell \boldsymbol{R}_\theta(s)ds + \frac{3}{\ell^2}\boldsymbol{R}_\theta(\ell) + \frac{6}{\ell^3}\boldsymbol{t}\left(\int_0^\ell \boldsymbol{R}_\theta(s)ds\right)\cdot\boldsymbol{t}\\
&= \frac{1}{2}\boldsymbol{\omega}''(0) + O(\ell^{1/2})\|\boldsymbol{\omega}'''\|_{L^2(0,\ell;\mathbb{R}^3)}
\end{aligned}$$

$$\boldsymbol{e} = \frac{\boldsymbol{\Theta}_\ell - \boldsymbol{\Theta}_0}{\ell} - \boldsymbol{d}\ell = \frac{1}{\ell}\left(\boldsymbol{\omega}'(0)\ell + \frac{1}{2}\boldsymbol{\omega}''(0)\ell^2 + \boldsymbol{R}_\theta(\ell)\right) - \ell\left(\frac{1}{2}\boldsymbol{\omega}''(0) + O(\ell^{1/2})\|\boldsymbol{\omega}'''\|_{L^2(0,\ell;\mathbb{R}^3)}\right)$$
$$= \boldsymbol{\omega}'(0) + \frac{1}{\ell}\boldsymbol{R}_\theta(\ell) + O(\ell^{3/2})\|\boldsymbol{\omega}'''\|_{L^2(0,\ell;\mathbb{R}^3)} = \boldsymbol{\omega}'(0) + O(\ell^{3/2})\|\boldsymbol{\omega}'''\|_{L^2(0,\ell;\mathbb{R}^3)}.$$

Here, the terms $O(\ell^{1/2})$ and $O(\ell^{3/2})$ are independent of the values of $(\boldsymbol{u}, \boldsymbol{\omega})$. Then,

$$\int_0^\ell |\boldsymbol{\omega}'(s) - \boldsymbol{\omega}^a{}'(s)|^2 ds = \int_0^\ell |\boldsymbol{\omega}'(s) - 2\boldsymbol{d}s - \boldsymbol{e}|^2 ds = \int_0^\ell |\boldsymbol{\omega}'(0) + \boldsymbol{\omega}''(0)s + O(\ell^{3/2})\|\boldsymbol{\omega}'''\|_{L^2}$$
$$- 2\left(\frac{1}{2}\boldsymbol{\omega}''(0) + O(\ell^{1/2})\|\boldsymbol{\omega}'''\|_{L^2}\right)s - \boldsymbol{\omega}'(0) + O(\ell^{3/2})\|\boldsymbol{\omega}'''\|_{L^2}|^2 ds$$
$$= \int_0^\ell |O(\ell^{3/2}) - 2O(\ell^{1/2})s|^2 ds \|\boldsymbol{\omega}'''\|_{L^2}^2 \le C\ell^4\|\boldsymbol{\omega}'''\|_{L^2}^2.$$

Using the standard technique, from the L^2 estimate for derivatives, we obtain the H^1 estimate. Namely, because $\boldsymbol{\omega}$ and $\boldsymbol{\omega}^a$ coincide at $s = 0$, using the Newton–Leibniz formula and the Cauchy–Schwartz inequality, we obtain

$$|\boldsymbol{\omega}(s) - \boldsymbol{\omega}^a(s)| = |\int_0^s (\boldsymbol{\omega}'(t) - \boldsymbol{\omega}^a{}'(s))ds| \le \sqrt{s}\|\boldsymbol{\omega}' - \boldsymbol{\omega}^a{}'\|_{L^2(0,\ell;\mathbb{R}^3)}.$$

Therefore,

$$\|\boldsymbol{\omega} - \boldsymbol{\omega}^a\|_{L^2(0,\ell;\mathbb{R}^3)}^2 \le \frac{\ell^2}{2}\|\boldsymbol{\omega}' - \boldsymbol{\omega}^a{}'\|_{L^2(0,\ell;\mathbb{R}^3)}^2 \le C\ell^6\|\boldsymbol{\omega}'''\|_{L^2(0,\ell;\mathbb{R}^3)}^2.$$

Using the inextensibility (19), we directly obtain the estimate for the approximation of $\boldsymbol{u}'$:

$$\|\boldsymbol{u}' - \boldsymbol{u}^a{}'\|_{L^2(0,\ell;\mathbb{R}^3)}^2 \le \|\boldsymbol{\omega} - \boldsymbol{\omega}^a\|_{L^2(0,\ell;\mathbb{R}^3)}^2 \le C\ell^6\|\boldsymbol{\omega}'''\|_{L^2(0,\ell;\mathbb{R}^3)}^2.$$

In a similar way as above, we then obtain the estimate

$$\|\boldsymbol{u} - \boldsymbol{u}^a\|_{L^2(0,\ell;\mathbb{R}^3)}^2 \le \frac{\ell^2}{2}\|\boldsymbol{u}' - \boldsymbol{u}^a{}'\|_{L^2(0,\ell;\mathbb{R}^3)}^2 \le C\ell^8\|\boldsymbol{\omega}'''\|_{L^2(0,\ell;\mathbb{R}^3)}^2.$$

Thus, we obtain the estimates for the difference of $\boldsymbol{u}_S|_{\boldsymbol{e}} = (\boldsymbol{u}, \boldsymbol{\omega})$ and $\boldsymbol{u}^a = (\boldsymbol{u}^a, \boldsymbol{\omega}^a)$

$$\begin{aligned} \|\boldsymbol{u}_S|_{\boldsymbol{e}} - \boldsymbol{u}^a\|_{L^2(0,\ell;\mathbb{R}^6)} &\le C\ell^3\|\boldsymbol{\omega}'''\|_{L^2(0,\ell;\mathbb{R}^3)}, \\ \|\boldsymbol{u}_S|_{\boldsymbol{e}} - \boldsymbol{u}^a\|_{H^1(0,\ell;\mathbb{R}^6)}^2 &\le C\ell^2\|\boldsymbol{\omega}'''\|_{L^2(0,\ell;\mathbb{R}^3)}. \end{aligned} \tag{27}$$

Let us now define the interpolation operator $\mathcal{I}^2$ (with polynomials of degree 2) on the stent

$$\mathcal{I}^2 : V_S^{\mathrm{Ker}} \cap L^2_{H^3}(\mathcal{N};\mathbb{R}^6) \to V_h^{\mathrm{Ker}}, \qquad (\mathcal{I}^2\boldsymbol{u}_S)|_{\boldsymbol{e}} := \boldsymbol{u}^a, \quad \boldsymbol{e} \in \mathcal{E}.$$

Lemma 2. *Let $h = \max\{\ell_i, i = 1 \dots, n_{\mathcal{E}}\}$. Then,*

$$\|\boldsymbol{u}_S - \mathcal{I}^2\boldsymbol{u}_S\|_{L^2(\mathcal{N};\mathbb{R}^6)} \le Ch^3\|\boldsymbol{\omega}'''\|_{L^2(\mathcal{N};\mathbb{R}^3)}, \quad \|\boldsymbol{u}_S - \mathcal{I}^2\boldsymbol{u}_S\|_{H^1(\mathcal{N};\mathbb{R}^6)} \le Ch^2\|\boldsymbol{\omega}'''\|_{L^2(\mathcal{N};\mathbb{R}^3)}, \tag{28}$$

for all $\boldsymbol{u}_S \in V_S^{\mathrm{Ker}} \cap L^2_{H^3}(\mathcal{N};\mathbb{R}^6)$.

Proof. At each edge $\boldsymbol{e}$, we fix the values of $\boldsymbol{u}_S$ at the ends of the edge. Then, we apply the construction from this section and, at the edge $\boldsymbol{e}$, construct the approximation $\boldsymbol{u}^a = (\boldsymbol{u}^a, \boldsymbol{\omega}^a)$ for which the estimates (27) hold. Summing these estimates, we obtain (28). In addition, note that the approximation on the whole stent made of such pieces belongs to $H^1(\mathcal{N};\mathbb{R}^6)$ and thus is in V_h^{Ker} as well. □

Remark 2. Note that, for given h, we can "virtually" add new vertices to the original network in order that all edges in the stent are of length not longer than h. Even though we obtain a new network, the equilibrium solutions for the same loadings of both structures are the same. This follows from the weak formulation of the problem and the kinematic coupling conditions, which correspond to the continuity in $H^1(\mathcal{N};\mathbb{R}^6)$.

In the rest of this subsection, we derive an error estimate for approximation of the Lagrange multiplier. It is a classical result that, for a function $\varphi \in H^k(0,\ell)$ and its polynomial Lagrange interpolant φ_m of degree m, one has the estimate (see, e.g., the work of Ciarlet[23])

$$\|\varphi - \varphi_m\|_{L^2(0,\ell)} \leq C\ell^{\min\{k,m+1\}} \|\varphi^{(\min\{k,m+1\})}\|_{L^2(0,\ell)}, \qquad \varphi \in H^k(0,\ell). \tag{29}$$

Because for piecewise quadratic elements we have h^2 estimate for $\boldsymbol{u}_S$ in Lemma 2, linear approximation is the natural choice for the multiplier $\boldsymbol{p}_S$. Then, applying this estimate on each edge, we obtain the following estimate.

Lemma 3. *Let $\boldsymbol{p}_S$ be such that $\boldsymbol{p}^i \in H^k(0,\ell_i;\mathbb{R}^3)$ for some $k \in \mathbb{N}$. Let $\mathcal{I}_n^1$ denotes the operator which to $\boldsymbol{p}_S$ assigns on each edge the linear Lagrange interpolation polynomial. Let $h = \max\{\ell_i, i = 1\dots, n_\mathcal{E}\}$. Then,*

$$\|\boldsymbol{p}_S - \mathcal{I}_n^1 \boldsymbol{p}_S\|_{L^2(\mathcal{N};\mathbb{R}^3)} \leq Ch^{\min\{k,2\}} \|\boldsymbol{p}_S^{(\min\{k,2\})}\|_{L^2(\mathcal{N};\mathbb{R}^3)}.$$

Remark 3. Building approximation piecewise (locally on separate edges) simplifies obtaining estimates greatly. However, the discrete inextensibility condition (21) is very restrictive. It turns out to be too restrictive for the first-order polynomials. Namely, solving a system following from the discrete inextensibility and (20) leads to the condition at the boundary values, which in general does not hold. Even if we split the interval in pieces and adjust the middle points, the problem remains.

Remark 4. Note that here it is also significant that we do not enforce the continuity of the multipliers, which both simplifies the analysis and has a positive effect on efficiency of computations because it reduces fill-ins.

3.4 | Rate of convergence

The discrete problem is given by the following. Find $(\boldsymbol{u}_S^h, \boldsymbol{p}_S^h) \in V_h \times Q_h$ such that

$$\begin{aligned} &k_S\left(\boldsymbol{u}_S^h, \tilde{\boldsymbol{u}}_S\right) + b_S\left(\boldsymbol{p}_S^h, \tilde{\boldsymbol{u}}_S\right) = l_S(\tilde{\boldsymbol{u}}_S), \quad \tilde{\boldsymbol{u}}_S \in V_h, \\ &b_S\left(\tilde{\boldsymbol{p}}_S, \boldsymbol{u}_S^h\right) = 0, \qquad \tilde{\boldsymbol{p}}_S \in Q_h. \end{aligned} \tag{30}$$

The following theorem gives the error estimate for the approximation.

Theorem 1. *Let $\boldsymbol{f} \in L^2_{H^1}(\mathcal{N};\mathbb{R}^3)$. Let $(\boldsymbol{u}_S, \boldsymbol{p}_S)$ be the solution of the problem (12) and $(\boldsymbol{u}_S^h, \boldsymbol{p}_S^h) \in V_h \times Q_h$ a solution of (17). Then,*

$$\left\|\boldsymbol{u}_S - \boldsymbol{u}_S^h\right\|_{V_S} \leq Ch^2 \left(\left\|\boldsymbol{u}_S'''\right\|_{L^2(\mathcal{N};\mathbb{R}^6)} + \left\|\boldsymbol{p}_S''\right\|_{L^2(\mathcal{N};\mathbb{R}^3)}\right).$$

Proof. By a direct computation, following the works of Boffi et al.,[11,15] we now obtain (the first inequality is obtained by V_S^{Ker} ellipticity of k_S from Lemma 1)

$$\begin{aligned} \left\|\boldsymbol{u}_S^h - \mathcal{I}^2\boldsymbol{u}_S\right\|_{V_S}^2 &\leq \frac{C}{\min_i \sigma(\mathbf{H}^i)} k\left(\boldsymbol{u}_S^h - \mathcal{I}^2\boldsymbol{u}_S, \boldsymbol{u}_S^h - \mathcal{I}^2\boldsymbol{u}_S\right) \\ &= \frac{C}{\min_i \sigma(\mathbf{H}^i)} \left(k_S\left(\boldsymbol{u}_S^h - \boldsymbol{u}_S, \boldsymbol{u}_S^h - \mathcal{I}^2\boldsymbol{u}_S\right) + k_S\left(\boldsymbol{u}_S - \mathcal{I}^2\boldsymbol{u}_S, \boldsymbol{u}_S^h - \mathcal{I}^2\boldsymbol{u}_S\right)\right) \\ &\leq \frac{C}{\min_i \sigma(\mathbf{H}^i)} \left|-b_S\left(\boldsymbol{p}_S^h - \boldsymbol{p}_S, \boldsymbol{u}_S^h - \mathcal{I}^2\boldsymbol{u}_S\right) + M_{k_S}\|\boldsymbol{u}_S - \mathcal{I}^2\boldsymbol{u}_S\|_{V_S}\left\|\boldsymbol{u}_S^h - \mathcal{I}^2\boldsymbol{u}_S\right\|_{V_S}\right|. \end{aligned}$$

From the second equation in (17), we have

$$b_S\left(\tilde{\boldsymbol{p}}_S, \boldsymbol{u}_S^h\right) = 0, \qquad \tilde{\boldsymbol{p}}_S \in Q_h.$$

From the construction of the interpolation operator $\mathcal{I}^2$, we also have

$$b_S\left(\tilde{\boldsymbol{p}}_S, \mathcal{I}^2\boldsymbol{u}_S\right) = 0, \qquad \tilde{\boldsymbol{p}}_S \in Q_h.$$

Thus, because $\mathcal{I}_n^1\boldsymbol{p}_S \in Q_h$, we have

$$b_S\left(\boldsymbol{p}_S^h, \boldsymbol{u}_S^h - \mathcal{I}^2\boldsymbol{u}_S\right) = b_S\left(\mathcal{I}_n^1\boldsymbol{p}_S, \boldsymbol{u}_S^h - \mathcal{I}^2\boldsymbol{u}_S\right) = 0.$$

Thus, using continuity of b on $Q_S \times V_S$, we obtain

$$\begin{aligned}\left\|\boldsymbol{u}_S^h - \mathcal{I}^2\boldsymbol{u}_S\right\|_{V_S}^2 &\leq \frac{C}{\min_i \sigma(\mathbf{H}^i)} |-b_S\left(\mathcal{I}_n^1\boldsymbol{p}_S - \boldsymbol{p}_S, \boldsymbol{u}_S^h - \mathcal{I}^2\boldsymbol{u}_S\right) + M_{k_S}\|\boldsymbol{u}_S - \mathcal{I}^2\boldsymbol{u}_S\|_{V_S}\left\|\boldsymbol{u}_S^h - \mathcal{I}^2\boldsymbol{u}_S\right\|_{V_S} \\ &\leq \frac{C}{\min_i \sigma(\mathbf{H}^i)}\left(M_{b_S}\|\mathcal{I}_n^1\boldsymbol{p}_S - \boldsymbol{p}_S\|_{L^2(\mathcal{N};\mathbb{R}^3)} + M_{k_S}\|\boldsymbol{u}_S - \mathcal{I}^2\boldsymbol{u}_S\|_{V_S}\right)\|\boldsymbol{u}_S^h - \mathcal{I}^2\boldsymbol{u}_S\|_{V_S}.\end{aligned}$$

Now, using Lemma 2 and Lemma 3, we estimate

$$\begin{aligned}\left\|\boldsymbol{u}_S - \boldsymbol{u}_S^h\right\|_{V_S} &\leq \|\boldsymbol{u}_S - \mathcal{I}^2\boldsymbol{u}_S\|_{V_S} + \left\|\mathcal{I}^2\boldsymbol{u}_S - \boldsymbol{u}_S^h\right\|_{V_S} \\ &\leq \|\boldsymbol{u}_S - \mathcal{I}^2\boldsymbol{u}_S\|_{V_S} + \frac{C}{\min_i \sigma(\mathbf{H}^i)}\left(M_{b_S}\left\|\boldsymbol{p}_S - \mathcal{I}_n^1\boldsymbol{p}_S\right\|_{L^2(\mathcal{N};\mathbb{R}^3)} + M_{k_S}\|\boldsymbol{u}_S - \mathcal{I}^2\boldsymbol{u}_S\|_{V_S}\right) \\ &\leq \left(1 + \frac{C}{\min_i \sigma(\mathbf{H}^i)}M_{k_S}\right)\|\boldsymbol{u}_S - \mathcal{I}^2\boldsymbol{u}_S\|_{V_S} + \frac{CM_{b_S}}{\min_i \sigma(\mathbf{H}^i)}\left\|\boldsymbol{p}_S - \mathcal{I}_n^1\boldsymbol{p}_S\right\|_{L^2(\mathcal{N};\mathbb{R}^3)} \\ &\leq \left(1 + \frac{C}{\min_i \sigma(\mathbf{H}^i)}M_{k_S}\right)Ch^2\left\|\boldsymbol{u}_S'''\right\|_{L^2(\mathcal{N};\mathbb{R}^6)} + \frac{CM_{b_S}}{\min_i \sigma(\mathbf{H}^i)}h^{\min\{k,3\}}\left\|\boldsymbol{p}_S^{(\min\{k,3\})}\right\|_{L^2(\mathcal{N};\mathbb{R}^3)} \\ &\leq Ch^2\left(\left\|\boldsymbol{u}_S'''\right\|_{L^2(\mathcal{N};\mathbb{R}^6)} + \left\|\boldsymbol{p}_S''\right\|_{L^2(\mathcal{N};\mathbb{R}^3)}\right)\end{aligned}$$

(in the last estimate, we use $k = 2$ because $\boldsymbol{f} \in L^2_{H^1}(\mathcal{N};\mathbb{R}^3)$ implies that $\boldsymbol{p}^i \in H^2(0,\ell_i)$). □

Essentially, using the discrete inextensibility of the interpolation, we are able to obtain the estimate

$$\left\|\boldsymbol{u}_S - \boldsymbol{u}_S^h\right\|_{V_S}^2 \leq C\left(\|\boldsymbol{u}_S - \mathcal{I}\boldsymbol{u}_S\|_{V_S}^2 + \|\boldsymbol{p}_S - \mathcal{I}^1\boldsymbol{p}_S\|_{L^2}^2\right).$$

Then, the interpolation properties give the error estimate.

Because we are missing the discrete inf sup inequality for b_S (i.e., on $V_h \times Q_h$), we do not have an estimate for $\|\boldsymbol{p}_S - \boldsymbol{p}_S^h\|_{L^2(\mathcal{N};\mathbb{R}^3)}$. However, in the numerical examples in the next section, the error of the approximation is behaving as expected.

3.5 | Discretization matrices

In this section, we will introduce the discretization matrices and discuss the efficiency of computation. We point a reader to the work of Arioli et al.,[9] which gives a unified treatment of discretizations of scalar differential operators on metric graphs. Given a graph $\mathcal{N} = (\mathcal{V},\mathcal{E})$, we define the degree $d(v) \in \mathbb{N}$ of a vertex $v \in \mathcal{V}$ as the number of edges $e \in \mathcal{E}$, which are incident with v. The maximum degree of the graph $\mathcal{N}$ is $d_{\max}(\mathcal{N}) := \max\{d(v) : v \in \mathcal{V}\}$. In the terminology of Arioli et al.,[9] starting from the initial graph $\mathcal{N} = (\mathcal{V},\mathcal{E})$, we create the extended graph $\mathcal{N}_h = (\mathcal{V}_h,\mathcal{E}_h)$, by introducing discretization nodes on the edges $e = [0,l_e]$, $e \in \mathcal{E}$ and then including the discretization nodes as new vertices in the graph $\mathcal{N}_h$ (cf. Remark 2). To complete the extended graph, we also add the edges, which connect the new vertex with its immediate geometric neighbors. The extended graph of the graph $\mathcal{N}$ is called its discretization.

According to remark 3.1 and theorem 3.3 of the work of Arioli et al.,[9] discretizing metric graphs in a vicinity of a vertex with a large degree might require adaptive mesh refinement to achieve sufficiently tight estimates for the interpolation operator in $H^1(\mathcal{N};\mathbb{R})$. On the other hand, in the vicinity of a vertex with low degree, uniform refinement strategies will yield satisfactory reduction of the approximation error. Recall that stent graphs have vertices with a degree at most four, and so uniform refinement can be expected to yield sufficient accuracy in a computationally efficient manner.

Motivated by the work of Arioli et al.,[9] in our subsequent experiments, we will use uniform refinement implemented by splitting the edges of the graph $\mathcal{N}$ in the edges of equal length. We will study the relationship between numerical efficiency and accuracy and the number k of uniform subdivisions of each edge. In this setting, we write $h = 1/k$ as the discretization parameter.

Note that we are studying systems of differential equations on a metric graph and so we are approximating vector-valued functions from $H^1(\mathcal{N};\mathbb{R}^6)$. Subsequently, our discretization matrices will have a global block structure dependent on the degree of the polynomials used in approximating spaces V_h and Q_h.

As a first example, let us consider an assembly of two struts, which we will be splitting $k = 16$ times to obtain $\mathcal{N}_{1/16}$.

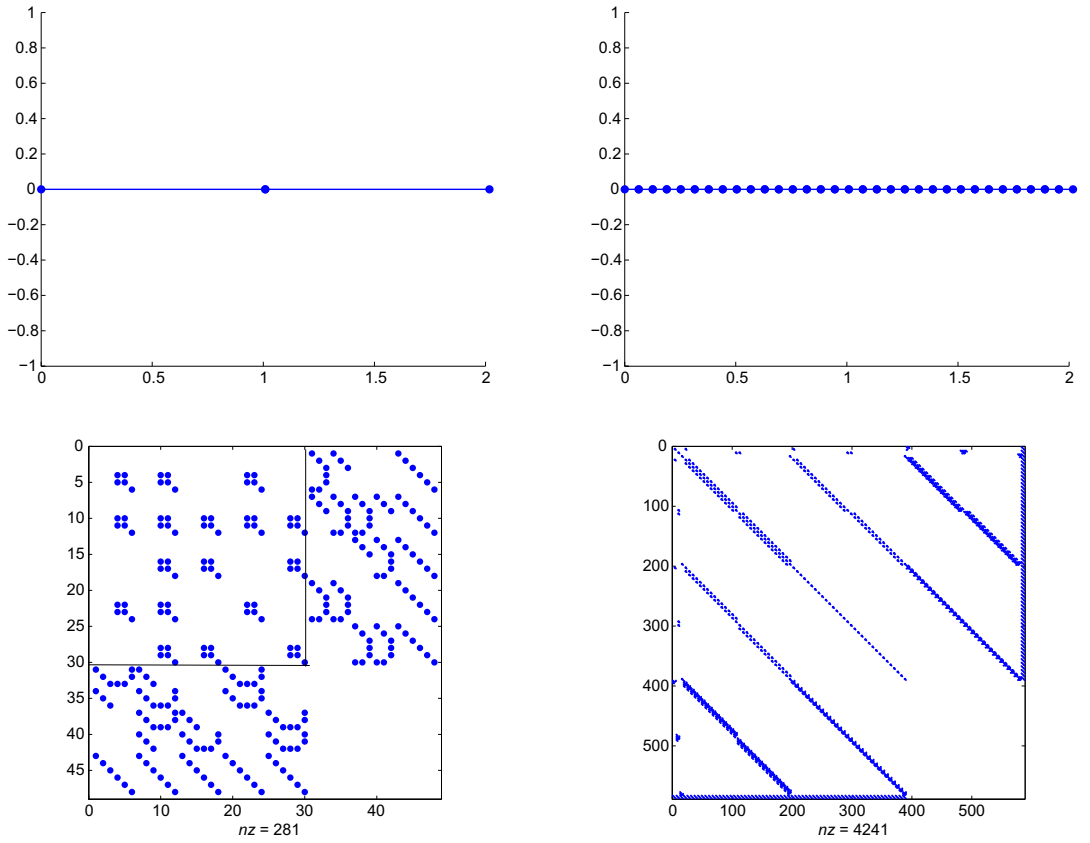

FIGURE 3 Symmetric saddle-point matrix A_1 for an assembly of two struts left and the matrix $A_{1/16}$ of the same assembly when we divide each of the struts in 16 subintervals, thus introducing more internal vertices

The space V_h is the space of continuous piecewise quadratic elements, and Q_h is the space of piecewise (not necessarily continuous) linear elements. The matrix

$$A_h = \begin{bmatrix} K_{S_h} & B_{S_h}^* \\ B_{S_h} & 0 \end{bmatrix},$$

which realizes (17) for this assembly, is presented in the left plot on Figure 3. These matrices have the structure of symmetric saddle-point matrices as is described in a comprehensive review.[7] The solution methods for such matrices are typically studied in the context of constrained optimization. For references, see other works.[12,24–27]

On the right-hand side plot in Figure 3, we see the structure of the matrix $A_{1/16}$ for the two-strut assembly when we divide each strut sixteen times. The discretization matrix corresponds to the extended graph, which in addition to the vertices of the original graph $\mathcal{N}$ contains the vertices associated to the midpoints of the edges (struts). This is incurred by the use of quadratic elements. The ordering of vertices in the extended graph is such that the vertices from $\mathcal{V}$ are numbered first and then come the midpoints of the edges (we will call them internal vertices). The last six rows and columns correspond to the multipliers $\boldsymbol{\alpha}$ and $\boldsymbol{\beta}$ necessary for obtaining uniqueness of the solution.

The discrete ellipticity from Lemma 1 implies $\ker(K_{S_h}) \cap \ker(B_{S_h}) = \{0\}$. Matrix A_h is invertible if and only if in addition $\ker(B_{S_h}^*)$ is trivial, which would be a consequence of the discrete inf sup condition. However, we have not been able to establish the inf sup condition a priori and so we will outline a method that will either compute the solution of the stationary problem or detect that the matrix $B_{S_h}^*$ has a nontrivial kernel.

Invertible symmetric saddle-point matrices have a diagonally pivoted block LDL^* factorization $P^*A_hP = LDL^*$ as described in the work of Duff.[10] Recall that the diagonal blocks in D are either 1×1 or 2×2 and L is unit lower triangular. Because we cannot assume that $\ker(B_{S_h}^*)$ is trivial, we have to rely on the rank-revealing pivoting strategies described in theorem 6 of the work of Fang[13] or the work of Reid et al.[14]

To summarize, we have the following result.

Lemma 4. *Let*

$$A_h = \begin{bmatrix} K_{S_h} & B_{S_h}^* \\ B_{S_h} & 0 \end{bmatrix}$$

be the matrix obtained by restricting the forms k_S and b_S from (17) to the spaces V_h and Q_h; then, there either exists a permutation matrix P, a lower triangular matrix L with ones on the diagonal, and an invertible block diagonal matrix D, where diagonal blocks are either 1×1 or 2×2 such that

$$P^* A_h P = LDL^*$$

or $\ker(B_{S_h}^*)$ *is not trivial.*

Proof. According to the work of Veselić et al.,[8] the kernel of A_h is

$$\ker(A_h) = \left\{ \begin{bmatrix} u_1 \\ u_2 \end{bmatrix} : u_1 \in \ker(K_{S_h}) \cap \ker(B_{S_h}),\ u_2 \in \ker\left(B_{S_h}^*\right) \right\}.$$

Now, Lemma 1 implies that $\ker(K_{S_h}) \cap \ker(B_{S_h})$ is trivial and so $\ker(A_h)$ is trivial—equivalently A_h is invertible—if and only if $\ker(B_{S_h}^*)$ is trivial. Because the LDL^* factorization with rook-like pivoting is rank revealing (see the works of Fang[13] and Reid et al.[14]), the block Gaussian elimination with rook-like pivoting will wither produce an invertible matrix D or it will detect $\operatorname{rank}(A_h) < \dim V_h + \dim Q_h$ and so A_h is not invertible. This is in turn equivalent to $\ker(B_{S_h}^*)$ being nontrivial as was claimed. □

To assess the efficiency of the solution of the stationary problem by the pivoted LDL^* decomposition, we will consider dependence of the number of nonzeros in the matrix L on the number of the subdivisions of the struts. We will consider the Cypher-like stent, inspired by the Cypher stent by Cordis, from Figure 1 and the Palmaz-like stent, inspired by the Palmaz stent also by Cordis, from Figure 8.

To assess what we expect as a possible fill-in in the matrix L, we present the following lemma.

Lemma 5. *Let the matrix A_h be associated to the discrete stent model obtained after $k = 1/h$ refinements of the graph $\mathcal{N}_h = (\mathcal{V}_h, \mathcal{E}_h)$. The number of nonzeros in a column of the matrix A_h associated to spaces $V_h \times Q_h$, where we use polynomials of degree m in V_h and polynomials of degree n in Q_h, is less than* $(3md_{\max}(\mathcal{N}_h) + 3) + 3(n+1)d_{\max}(\mathcal{N}_h) + 1$.

Proof. Proof follows by considering the block structure of the matrices K_{S_h} and B_{S_h}. Let $n_{v,h} = \operatorname{card}(\mathcal{V}_h)$ be the number of vertices in the graph $\mathcal{N}_h$ and $n_{e,h} = \operatorname{card}(\mathcal{E}_h)$ the number of edges. The dimension of the matrix K_{S_h} is $(6n_{v,h} + 6n_{e,h}(m-1)) \times (6n_{v,h} + 6n_{e,h}(m-1))$ and the dimension of the matrix B_{S_h} is $(3(n+1)n_{e,h} + 6) \times (6n_{v,h} + 6n_{e,h}(m-1))$.

The first part of the estimate follows from K_{S_h} where in each column—corresponding to the vertex—we have in each block column $3m$ nonzeros corresponding to each vertex, which is a direct neighbor of the given vertex.

The second part follows from the inextensibility condition, which incurs a block of nonzero elements in matrix B_{S_h} for each vertex (represented by the rows of the matrix), which is incident with a given edge.

The last part comes from the global restriction on the center of the mass, which is a diagonal matrix that adds precisely one nonzero element in each column. □

The matrix L produced by rook pivoting is going to be sparse due to the fact that stent graphs have vertices with low maximal vertex degrees (typically less than four). On the other hand, the fill-in that appears is due to the global equations, which the multipliers $\boldsymbol{\alpha}$ and $\boldsymbol{\beta}$ satisfy in order to realize the uniqueness of the solution. For instance, in the case of two rods from Figure 3, the last six rows in the matrix B_{S_1} correspond to the multipliers $\boldsymbol{\alpha}$ and $\boldsymbol{\beta}$ from Section 2.3.

The sparsity pattern for the matrix A and the lower triangular L for the Palmaz-like stent are presented in Figure 4. We will use the Palmaz-like stent for the numerical validation of the method in Section 4.

Finally, we empirically study the relationship between the fill-in—measured as the percentage of nonzero elements in the matrix—against the number of times each edge has been split. The model of the Cypher-like stent had more degrees of freedom initially, but the increase in the degrees of freedom with refinement leads to the smaller final matrix $A_{1/16}$.

We see that, in both cases, the fill-in was decreasing with the number of subdivisions; see Figures 5 and 6. Finally, we compare the fill for both stents on the same plot against the number of the degrees of freedom (the dimension of the matrices $A_{1/k}$, $k = 1, 2, 4, 8, 16$). We see that in both cases—characterized by the low maximal degree of the vertices in the underlying metric graphs—the fill-in decays with the refinement at the same exponential rate (see Figure 7).

Let us point out how to obtain algorithmic alternatives to the use of pivoted indefinite block LDL^* factorization as implemented in the routine `MA57` from the work of Duff.[10] For alternative methods that preserve symmetry, see the work

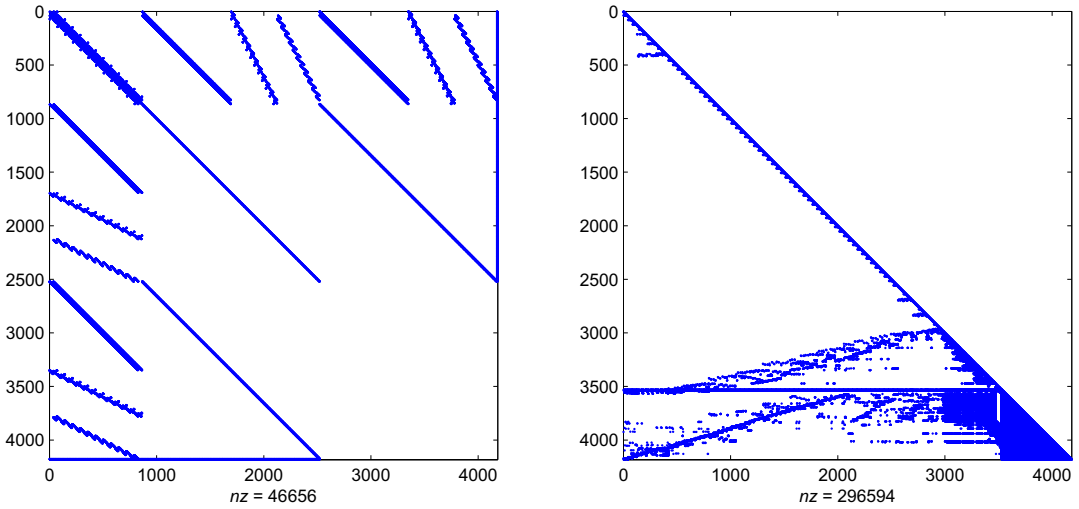

FIGURE 4 Sparsity pattern of the L matrix for the Palmaz-like stent. The original metric graph of the stent has 276 edges

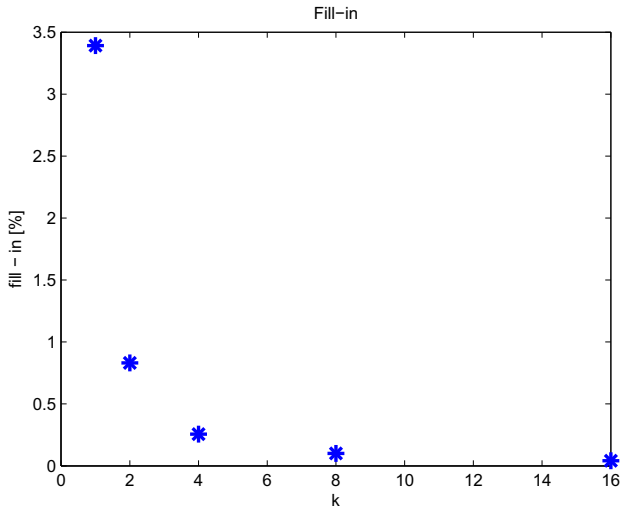

FIGURE 5 The decay of the fill-in for the Palmaz-like stent

of Gill et al.,[12] where they analyze the stability of the LDL^* factorization (here, D is a diagonal matrix with both positive and negative diagonal elements) for quasidefinite matrices. Note that our matrix is not quasidefinite in the sense of the work of Gill et al.[12] Alternatively, we might consider ignoring symmetry and applying a pivoted sparse LU factorization directly.[28] To this end, consider the discretization matrix*

$$A'_h = \begin{bmatrix} K_{S_h} & B^*_{S_h} \\ B_{S_h} & -h^2 M_{Q_h} \end{bmatrix}, \tag{31}$$

where M_{Q_h} is the mass matrix in the Q_h space and B_{S_h} and K_{S_h} are as in Lemma 4. This matrix is obviously invertible under the conditions on the block coefficients from Lemma 4, namely, $\ker(K_{S_h}) \cap \ker(B_{S_h}) = \emptyset$ and M_{Q_h} invertible, and so we can even apply a sparse pivoted LU factorization-based algorithm to it; see the work of Davis.[28] If an application of an LDL^* factorization is intended, then we need to imply further stabilization as in section 6.1. of the work of Gill et al.[12]; see Remark 6. Note that, following theorem 1 of the work of Vanderbei,[27] the inverse of this matrix is a quasidefinite matrix. In summary, we have the following result relating the matrices A_h and A'_h.

*The use of the stabilized matrix in this context has been suggested to the authors by an anonymous referee. We are thankful for this suggestion.

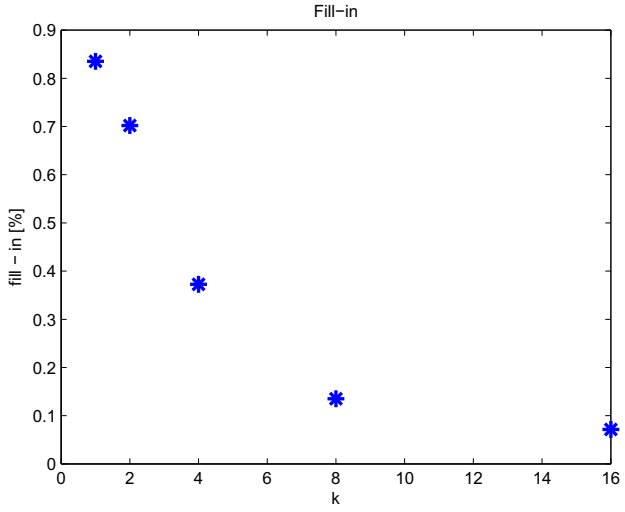

FIGURE 6 The decay of the fill-in for the Cypher-like stent

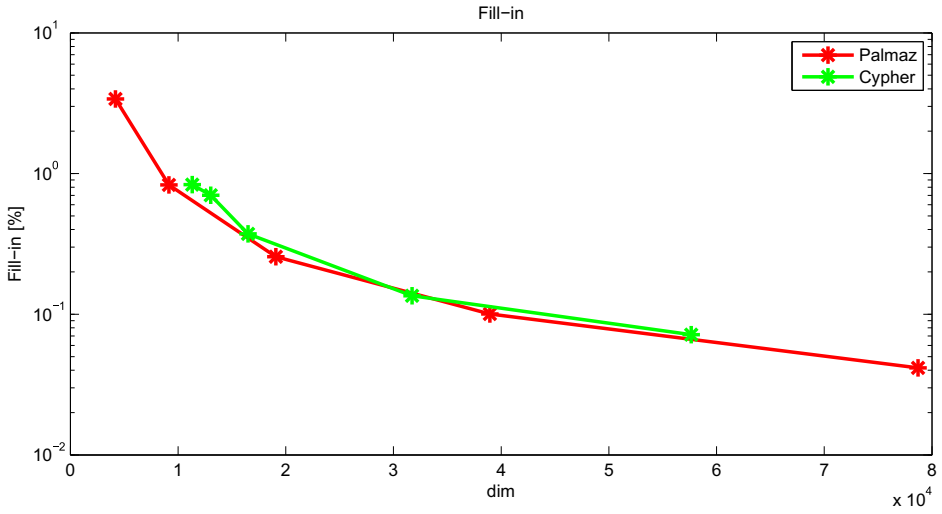

FIGURE 7 A logarithmic plot of the decay of fill-in with refinement for the Palmaz-like and the Cypher-like stents. Note that the sizes of the matrices are typically less than 50,000 DOF to achieve the accuracy warranted by the model

Lemma 6. *Let* u_h, u'_h, p_h, *and* p'_h *be such that*

$$\begin{bmatrix} K_{S_h} & B^*_{S_h} \\ B_{S_h} & 0 \end{bmatrix} \begin{bmatrix} u_h \\ p_h \end{bmatrix} = \begin{bmatrix} f \\ 0 \end{bmatrix}, \quad A'_h = \begin{bmatrix} K_{S_h} & B^*_{S_h} \\ B_{S_h} & -h^2 M_{Q_h} \end{bmatrix} \begin{bmatrix} u'_h \\ p'_h \end{bmatrix} = \begin{bmatrix} f \\ 0 \end{bmatrix}. \tag{32}$$

Set $K_1 = (K_{S_h} + B^*_{S_h} M^{-1}_{Q_h} B_{S_h})$, *then*

$$u_h - u'_h = \left(K_{S_h} + h^{-2} B^*_{S_h} M^{-1}_{Q_h} B_{S_h}\right)^{-1} B^*_{S_h} p_h,$$

and for h, $0 < h < 1$,

$$\left\| \left(K_{S_h} + h^{-2} B^*_{S_h} M^{-1}_{Q_h} B_{S_h}\right)^{-1} \right\| \leq h^2 \left(\left\| \left(B_{S_h} K_1^{-1/2}\right)^+ \right\| + h^2 \right) \left\| K_1^{-1} \right\|.$$

Here, $(B_{S_h} K_1^{-1/2})^+$ *denotes the Moore–Penrose pseudoinverse.*

Proof. This result can be obtained using proposition 4.3.3 of the work of Boffi et al.[11] However, we provide an alternative direct proof using a technique motivated by the work of Vanderbei.[27] Starting from (32), we obtain

$$\begin{bmatrix} K_{S_h} & B_{S_h}^* \\ B_{S_h} & -h^2 M_{Q_h} \end{bmatrix} \begin{bmatrix} u_h - u_h' \\ p_h - p_h' \end{bmatrix} = \begin{bmatrix} 0 \\ -h^2 M_{Q_h} p_h \end{bmatrix},$$

from which using Gaussian block elimination we get the first identity

$$u_h - u_h' = \left(K_{S_h} + h^{-2} B_{S_h}^* M_{Q_h}^{-1} B_{S_h} \right)^{-1} B_{S_h}^* p_h \quad .$$

To estimate the norm, we start form the decomposition

$$\begin{aligned} \left(K_{S_h} + h^{-2} B_{S_h}^* M_{Q_h}^{-1} B_{S_h} \right)^{-1} &= h^2 \left(h^2 K_{S_h} + B_{S_h}^* M_{Q_h}^{-1} B_{S_h} \right)^{-1} \\ &= h^2 \left(h^2 \left(K_{S_h} + B_{S_h}^* M_{Q_h}^{-1} B_{S_h} \right) + (1 - h^2) B_{S_h}^* M_{Q_h}^{-1} B_{S_h} \right)^{-1} \\ &= h^2 K_1^{-1/2} \left(h^2 I + (1 - h^2) K_1^{-1/2} B_{S_h}^* M_{Q_h}^{-1} B_{S_h} K_1^{-1/2} \right)^{-1} K_1^{-1/2} \quad . \end{aligned}$$

The matrices (operators) are Hermitian and positive definite, and so by Weyl's eigenvalue perturbation theorem, we compute the estimate. □

Corollary 1. *Let* $(\boldsymbol{u}_S, \boldsymbol{p}_S)$ *be the solution of the problem (12) and* $(\boldsymbol{u}_S^{h'}, \boldsymbol{p}_S^{h'}) \in V_h \times Q_h$ *be an approximation computed from (31). Then,*

$$\left\| \boldsymbol{u}_S - \boldsymbol{u}_S^{h'} \right\|_{V_S} \leq C h^2 \left(\left\| \boldsymbol{u}_S''' \right\|_{L^2(\mathcal{N};\mathbb{R}^6)} + \left\| \boldsymbol{p}_S'' \right\|_{L^2(\mathcal{N};\mathbb{R}^3)} \right) + C_2 h^2.$$

The constant C_2 *depends on* $\|(B_{S_h} K_1^{-1/2})^+\|$, $\|K_1^{-1/2}\|$ *and* $\| \boldsymbol{f} \|_2$.

Remark 5. Note that depending on the use of the stabilization, we will either use pivoted block LDL^* factorization as in conjunction with the result of Lemma 4 or pivoted LU or LDL^* (here, D is diagonal) decomposition applied on the stabilized matrix A_h' from Lemma 6. The accuracy of the approximation $\boldsymbol{u}_S^h$ or $\boldsymbol{u}_S^{h'}$ will be in both cases on the order of the discretization error; however, performance of the numerical schemes might differ. Note that, in the case in which the inf sup for the form b_S restricted to the discrete space $Q_h \times V_h$ can be bounded independent of h, we can obtain a bound independent of h for $\|(B_{S_h} K_1^{-1/2})^+\|$. Similarly, if the discrete ellipticity constant is independent of h, then $\|K_1^{-1/2}\|$ can also be bounded independent of h. For some technical details, see section 4.3 of the work of Arioli.[24] In this case, we were not able to obtain such bounds due to the fact that the restrictions imposed by the inextensibility conditions in the discrete space of a stent are posing a considerable technical restriction. Alleviating this will be the topic of further research.

Remark 6. If an application of an LDL^* decomposition is desired, then one should consider, following section 6.1 of the work of Gill et al.,[12] further stabilization

$$A_h'' = \begin{bmatrix} K_{S_h} + h^2 T_{S_h} & B_{S_h}^* \\ B_{S_h} & -h^2 M_{Q_h} \end{bmatrix}, \tag{33}$$

where T_{S_h} is the discretization of the form $m_S : V_S \times V_S \to \mathbb{R}$,

$$m_S(\boldsymbol{u}_S, \tilde{\boldsymbol{u}}_S) = \sum_{i=1}^{n_E} \int_0^{\ell_i} \|\mathbf{H}_i\|_F \left(\boldsymbol{u}^i \cdot \tilde{\boldsymbol{u}}^i + \boldsymbol{\omega}_i \cdot \tilde{\boldsymbol{\omega}}^i \right) ds;$$

here, $\|\mathbf{H}_i\|_F$ is the Frobenius norm of matrix $\mathbf{H}_i$ describing the material propertied of the rod i. This is the mass matrix in V_{S_h} and $K_{S_h} + h^2 T_{S_h}$ is positive definite for any h, $h > 0$. The matrix A_{S_h}'' is symmetric quasidefinite and the analysis of other works[12,24,27] applies directly. Note that the inequality—in the sense of Loewner—

$$\left(K_{S_h} + h^{-2} B_{S_h}^* M_{Q_h}^{-1} B_{S_h} \right) \leq \left(K_{S_h} + h^2 T_{S_h} + h^{-2} B_{S_h}^* M_{Q_h}^{-1} B_{S_h} \right)$$

implies

$$\left(K_{S_h} + h^2 T_{S_h} + h^{-2} B_{S_h}^* M_{Q_h}^{-1} B_{S_h} \right)^{-1} \leq \left(K_{S_h} + h^{-2} B_{S_h}^* M_{Q_h}^{-1} B_{S_h} \right)^{-1} = O(h^2)$$

and so the main identity reads

$$u_h - u_h'' = \left(K_{S_h} + h^2 T_{S_h} + h^{-2} B_{S_h}^* M_{Q_h}^{-1} B_{S_h}\right)^{-1} \left(B_{S_h}^* p_h - h^2 T_{S_h} u_h\right)$$

and then

$$\left\| \boldsymbol{u}_S - \boldsymbol{u}_S^{h''} \right\|_{V_S} \leq Ch^2 \left(\left\| \boldsymbol{u}_S''' \right\|_{L^2(\mathcal{N};\mathbb{R}^6)} + \left\| \boldsymbol{p}_S'' \right\|_{L^2(\mathcal{N};\mathbb{R}^3)} \right) + C_2'' h^2 \tag{34}$$

follows under the same condition as the result of Corollary 1. The condition number of the quasidefinite system will be, according to section 6.1 of the work of Gill et al.,[12] $O(h^{-2})$. Because we do not expect to be making many refinements, this provides a further algorithmic alternative to the use of block LDL^* decomposition and its ramifications will be exploited in the context of a follow-up paper on the eigenvalue problem. Note that any diagonal permutation of a quasidefinite matrix has an LDL^* factorization and so one might mix pivoting strategies that control stability with those that control the fill-in safely; see the work of Gill et al.[12]

Remark 7. In the case in which the solution of the stationary problem is used inside a parametrized stent topology optimization loop, it is of course of interest to solve the problem numerically as efficiently as possible. In this context, it might be of interest to use iterative solution methods, particularly those that can provably converge in few iterations, which is frequently the case for quasidefinite matrices.[24–26,29,30] Note that the matrices which we produce are degenerate quasidefinite matrices in that the leading diagonal block is no longer positive definite but positive semidefinite. However, the displacement vector u_h that we compute is always unique and it is for the costate p_h where we lack uniqueness. The methods from the work of Arioli[24] have been explored in this context in the work of Arioli et al.[31] There, starting from the system (32), one constructs an equivalent system; see equation (1.6) of the work of Arioli et al.[31] for an argument,

$$\begin{bmatrix} K_{S_h} + h^{-2} B_{S_h}^* M_{Q_h}^{-1} B_{S_h} & B_{S_h}^* \\ B_{S_h} & 0 \end{bmatrix} \begin{bmatrix} u_h \\ p_h \end{bmatrix} = \begin{bmatrix} 0 \\ b \end{bmatrix}, \qquad b = -B_{S_h} \left(K_{S_h} + h^{-2} B_{S_h}^* M_{Q_h}^{-1} B_{S_h}\right)^{-1} f \quad .$$

Note that the matrix $W = K_{S_h} + h^{-2} B_{S_h}^* M_{Q_h}^{-1} B_{S_h}$ is symmetric and positive definite. Following the work of Arioli et al.,[31] one constructs a further equivalent system by bidiagonalizing the matrix $B_{S_h}^*$ in the W dependent scalar product to obtain

$$B_{S_h}^* Q = WV \begin{bmatrix} \tilde{B} \\ 0 \end{bmatrix},$$

where $\tilde{B}$ is a bidiagonal matrix and matrices V and Q are W and $h^2 M_{Q_h}$ orthogonal, respectively. With this, we obtain an equivalent, after the change of variables, system (for further details, see the work of Arioli et al.[31])

$$\begin{bmatrix} I & \tilde{B}^* \\ \tilde{B} & 0 \end{bmatrix} \begin{bmatrix} x \\ y \end{bmatrix} = \begin{bmatrix} 0 \\ Q^* b \end{bmatrix}$$

whose minimum norm solution is uniquely determined and can be found in linear (in the dimension of the system) time. Because the first component of the solution is unique, this yields—after the change of variables—the uniquely determined displacement vector u_h. How to construct iterative methods for solving systems involving matrices of this form has also been discussed in the work of Arioli et al.[31] (and the references therein). Note however that the matrix W is potentially no longer sparse. An alternative would be to apply the method of the work of Arioli et al.[31] and, in particular, the bidiagonalization approach, which we just described, to the stabilized matrix

$$A_h''' = \begin{bmatrix} K_{S_h} + h^2 T_{S_h} & B_{S_h}^* \\ B_{S_h} & 0 \end{bmatrix} \tag{35}$$

and the standard right-hand side. The matrix $K_{S_h} + h^2 T_{S_h}$ is now sparse and the perturbation argument from Remark 6 still applies so that we can relate the solution u_h''' of the stabilized system with system matrix (35) to u_h and, thus, to u. Key observations[†] are that the displacement vectors u and u_h are unique, and we may use an efficient algorithm to compute a minimum norm solution from which we discard p_h''' and keep u_h'''.These observations will be a base for developing iterative computational schemes, which are going to be a topic of further research.

[†]We are very thankful to an anonymous referee for impressing importance of this observation on us and for pointing out the reference.[31]

4 | NUMERICAL EXAMPLES

We test and validate the implementation of the numerical scheme on the Palmaz-type stent on Figure 8. The radius of the stent is 1.5 mm and the overall length is 1.68 cm. There are 144 vertices in the associated graph with 276 edges, which are all straight. All vertices except the boundary ones are junctions of four edges. The cross-sections are assumed to be square with the side length 0.1mm. The material of the stent to be stainless steel with Young's modulus $E = 2.1 \cdot 10^{11}$ and Poisson's ratio $\nu = 0.26506$. At this structure, we apply the forcing of the form

$$\boldsymbol{f}(\boldsymbol{x}) = f(x_1)\frac{x_2\boldsymbol{e}_2 + x_3\boldsymbol{e}_3}{\sqrt{x_2^2 + x_3^2}}, \qquad \boldsymbol{x} = (x_1, x_2, x_3) \in \mathbb{R}^3$$

for two choices of the scalar functions f. Therefore, the applied forcing is radial with respect to the cylinder of the stent, with x_1 being the longitudinal variable of the stent. As a consequence, the deformation will also posses some radial symmetry. Because we assume the stent is nowhere fixed, the problem is of the pure traction form. However the applied forcing satisfies the necessary condition, and the nonuniqueness of the solution in the problem is fixed using the Lagrange multipliers.

The solution for constant function

$$f(x_1) = 2500$$

is given in Figure 9, whereas for quadratic

$$f(x_1) = 25000000x_1^2,$$

the solution is plotted in Figure 10.

In the sequel, we present the order of convergence of the applied method for the solution of the problem with the quadratic forcing. We divide all the edges on 128 smaller rods, and for this discretization, we solve the equilibrium

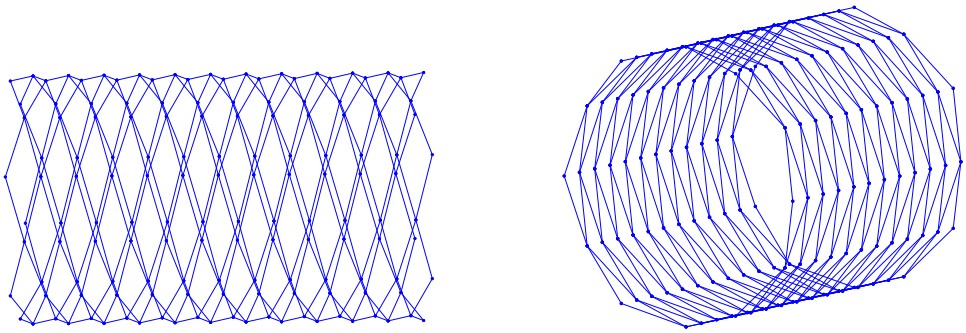

FIGURE 8 Design of the Palmaz-like stent used in simulations

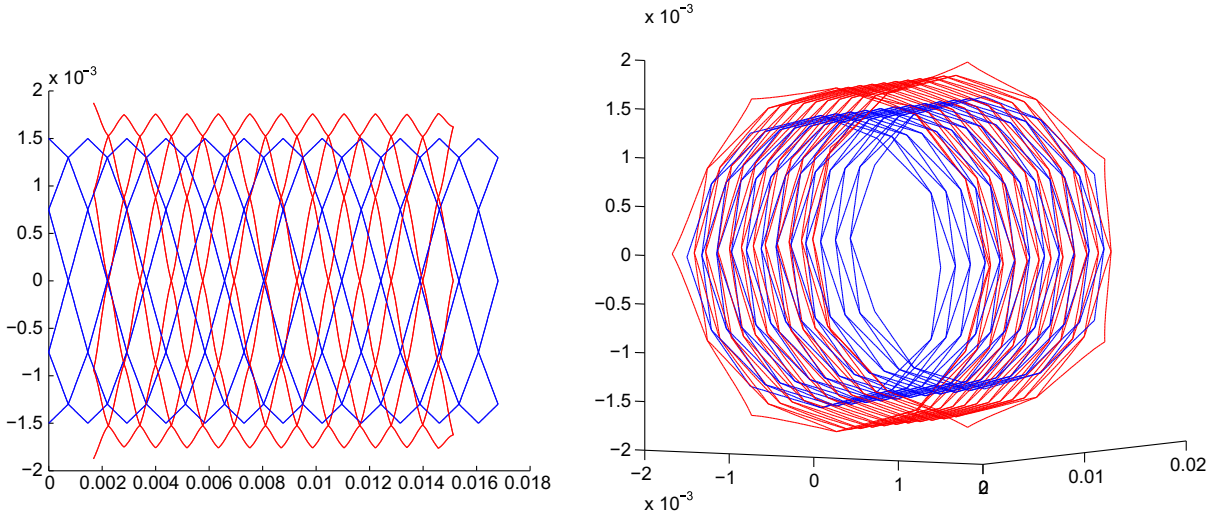

FIGURE 9 Solution for the constant radial load

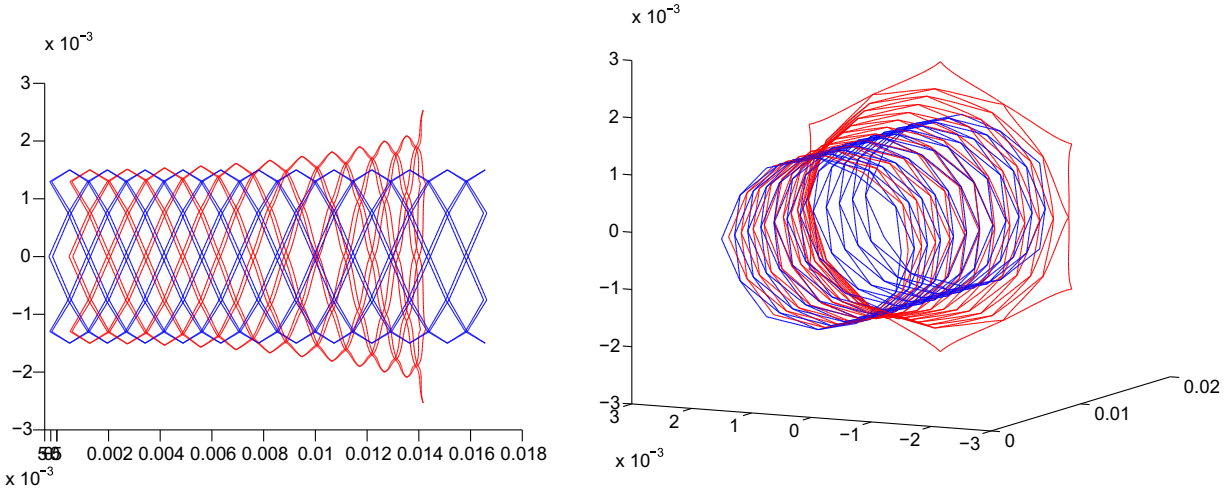

FIGURE 10 Solution for the radial force quadratic with respect to the length of the stent

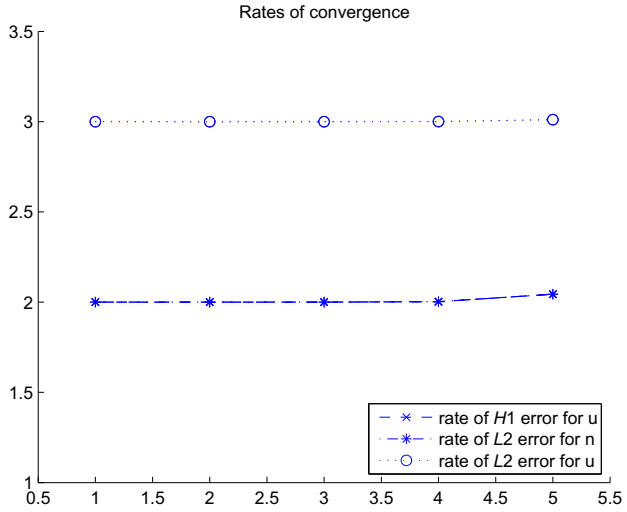

FIGURE 11 Rate of convergence for the displacement/rotations and Lagrange multipliers using P^2-P^1 elements

problem. We consider the obtained solution $\boldsymbol{u}_S, \boldsymbol{p}_S$ as the "exact" one. Then, we solve the equilibrium problem for all edges split in 2^i smaller rods, $i = 1, \ldots, 6$, that is, for smaller rods of length

$$h = 10^{-3} \cdot (0.5331, 0.2665, 0.1333, 0.0666, 0.0333, 0.0166)$$

and obtain the approximate solutions $(\boldsymbol{u}_S^i, \boldsymbol{p}_S^i)$, $i = 1, \ldots, 6$. Then, we obtain the errors

$$E_i^{\boldsymbol{u}} = \left\| \boldsymbol{u}_S^i - \boldsymbol{u}_S \right\|_{H^1(\mathcal{N};\mathbb{R}^6)}, \qquad E_i^{\boldsymbol{p}} = \left\| \boldsymbol{p}_S^i - \boldsymbol{p}_S \right\|_{L^2(\mathcal{N};\mathbb{R}^6)}, \qquad i = 1, \ldots, 6.$$

Finally, we calculate the numbers

$$\alpha_i^{\boldsymbol{u}} = \frac{\log \frac{E_{i+1}^{\boldsymbol{u}}}{E_i^{\boldsymbol{u}}}}{\log \frac{h_{i+1}}{h_i}}, \qquad \alpha_i^{\boldsymbol{p}} = \frac{\log \frac{E_{i+1}^{\boldsymbol{p}}}{E_i^{\boldsymbol{p}}}}{\log \frac{h_{i+1}}{h_i}}, \qquad = 1, \ldots, 5.$$

These two numbers, together with the rate of L^2 error for $\boldsymbol{u}_S$, are plotted with respect to i in Figure 11 for the choice of P^2 polynomials for $\boldsymbol{u}_S$ and P^1 polynomials for $\boldsymbol{p}_S$.

In the case of the choice of P^3 polynomials for $\boldsymbol{u}_S$ and P^2 polynomials for $\boldsymbol{p}_S$, the rates are plotted in Figure 12. The rates of convergence are for one order greater than in the quadratic-linear approximation, as expected.

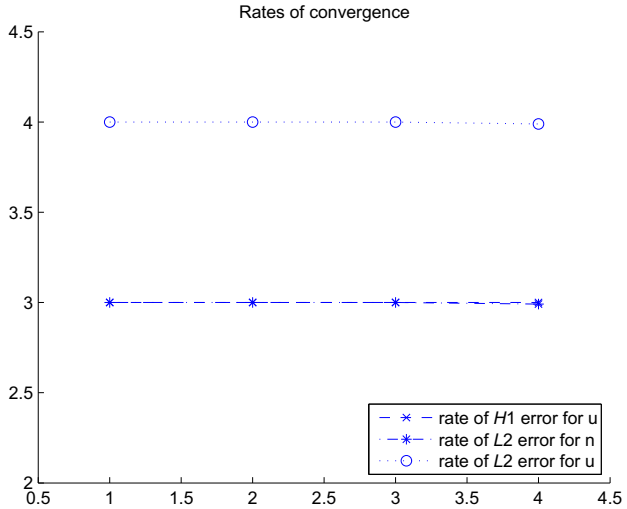

FIGURE 12 Rate of convergence for the displacement/rotations and Lagrange multipliers using P^3-P^2 elements

ACKNOWLEDGEMENTS

The work of the first author has been supported by Grant HRZZ9345 of the Croatian Science Foundation. We gratefully acknowledge the support. We are also thankful to the anonymous referee for the advice regarding the numerical linear algebra of quasidefinite matrices. It improved this paper significantly.

ORCID

Luka Grubišić https://orcid.org/0000-0002-3370-9353
Josip Tambača https://orcid.org/0000-0003-1792-6056

REFERENCES

1. Jurak M, Tambača J. Derivation and justification of a curved rod model. Math Models Methods Appl Sci. 1999;9(7):991–1014. Available from: https://doi.org/10.1142/S0218202599000452
2. Jurak M, Tambača J. Linear curved rod model: general curve. Math Models Methods Appl Sci. 2001;11(7):1237–1252. Available from: https://doi.org/10.1142/S0218202501001318
3. Tambača J, Kosor M, Čanić S, Paniagua D. Mathematical modeling of vascular stents. SIAM J Appl Math. 2010;70(6):1922–1952. Available from: https://doi.org/10.1137/080722618
4. Čanić S, Tambača J. Cardiovascular stents as PDE nets: 1D vs. 3D. IMA J Appl Math. 2012;77(6):748–770. Available from: https://doi.org/10.1093/imamat/hxs047
5. Griso G. Asymptotic behavior of structures made of curved rods. Anal Appl. 2008;6(1):11–22. Available from: https://doi.org/10.1142/S0219530508001031
6. Grubišić L, Iveković J, Tambača J, Žugec B. Mixed formulation of the one-dimensional equilibrium model for elastic stents. Rad Hrvat Akad Znan Umjet Mat Znan. 2017;21(532):219–240.
7. Benzi M, Golub GH, Liesen J. Numerical solution of saddle point problems. Acta Numerica. 2005;14:1–137. Available from: https://doi.org/10.1017/S0962492904000212
8. Veselić Ivan, Veselić K. Spectral gap estimates for some block matrices. Oper Matrices. 2015;9(2):241–275. Available from: https://doi.org/10.7153/oam-09-15
9. Arioli M, Benzi M. A finite element method for quantum graphs. IMA J Numer Anal. 2018;38(3):1119–1163. Available from: https://doi.org/10.1093/imanum/drx029
10. Duff IS. MA57—a code for the solution of sparse symmetric definite and indefinite systems. ACM Trans Math Softw. 2004;30(2):118–144. Available from: https://doi.org/10.1145/992200.992202
11. Boffi D, Brezzi F, Fortin M. Mixed finite element methods and applications. Berlin, Germany: Springer; 2013. Springer series in computational mathematics, No. 44. Available from: https://doi.org/10.1007/978-3-642-36519-5
12. Gill PE, Saunders MA, Shinnerl JR. On the stability of Cholesky factorization for symmetric quasidefinite systems. SIAM J Matrix Anal Appl. 1996;17(1):35–46. Available from: https://doi.org/10.1137/S0895479893252623

13. Fang H. Stability analysis of block LDL^T factorization for symmetric indefinite matrices. IMA J Numer Anal. 2011;31(2):528–555. Available from: https://doi.org/10.1093/imanum/drp053
14. Reid JK, Scott JA. Partial factorization of a dense symmetric indefinite matrix. ACM Trans Math Softw. 2011;38(2). Available from: https://doi.org/10.1145/2049673.2049674
15. Boffi D, Brezzi F, Gastaldi L. On the convergence of eigenvalues for mixed formulations. Ann Scuola Norm Sup Pisa Cl Sci. 1997;25(1–2):131–154. Dedicated to Ennio De Giorgi. Available from: http://www.numdam.org/item?id=ASNSP_1997_4_25_1-2_131_0
16. Cao DQ, Tucker RW. Nonlinear dynamics of elastic rods using the Cosserat theory: modelling and simulation. Int J Solids Struct. 2008;45(2):460–477. Available from: http://www.sciencedirect.com/science/article/pii/S0020768307003253
17. Antman SS. Nonlinear problems of elasticity. 2nd ed. New York, NY: Springer; 2005. Applied mathematical sciences, No. 107.
18. Kosor M, Tambača J. Nonlinear bending-torsion model for curved rods with little regularity. Math Mech Solids. 2017;22(4):708–717. Available from: https://doi.org/10.1177/1081286515608910
19. Tambača Josip. A model of irregular curved rods. In: Applied mathematics and scientific computing. Boston, MA: Springer; 2003. p. 289–299.
20. Tambača J, Velčić I. Derivation of the nonlinear bending-torsion model for a junction of elastic rods. Proc Roy Soc Edinburgh Sect A. 2012;142(3):633–664. Available from: https://doi.org/10.1017/S0308210510000491
21. Tambača J, Žugec B. One-dimensional quasistatic model of biodegradable elastic curved rods. Z Angew Math Phys. 2015;66(5):2759–2785. Available from: https://doi.org/10.1007/s00033-015-0512-3
22. Girault V, Raviart P-A. Finite element approximation of the Navier-Stokes equations. Berlin, Germany: Springer-Verlag Berlin Heidelberg; 1979. Lecture notes in mathematics, No. 749.
23. Ciarlet PG. The finite element method for elliptic problems. Philadelphia, PA: SIAM; 2002. Classics in applied mathematics, No. 40. Reprint of the 1978 original [North-Holland, Amsterdam; MR0520174 (58 #25001)]. Available from: https://doi.org/10.1137/1.9780898719208
24. Arioli M. Generalized Golub-Kahan bidiagonalization and stopping criteria. SIAM J Matrix Anal Appl. 2013;34(2):571–592. Available from: https://doi.org/10.1137/120866543
25. Orban D, Arioli M. Iterative solution of symmetric quasi-definite linear systems. Philadelphia, PA: SIAM; 2017. SIAM spotlights, No. 3.
26. Siefert C, de Sturler E. Preconditioners for generalized saddle-point problems. SIAM J Numer Anal. 2006;44(3):1275–1296. Available from: https://doi.org/10.1137/040610908
27. Vanderbei RJ. Symmetric quasidefinite matrices. SIAM J Optim. 1995;5(1):100–113. Available from: https://doi.org/10.1137/0805005
28. Davis TA. Direct methods for sparse linear systems. Philadelphia, PA: SIAM; 2006. Fundamentals of algorithms, No. 2. Available from: https://doi.org/10.1137/1.9780898718881
29. Benzi M, Golub GH. A preconditioner for generalized saddle point problems. SIAM J Matrix Anal Appl. 2004;26(1):20–41. Available from: https://doi.org/10.1137/S0895479802417106
30. Krzyżanowski P. On block preconditioners for saddle point problems with singular or indefinite (1, 1) block. Numer Linear Algebra Appl. 2011;18(1):123–140. Available from: https://doi.org/10.1002/nla.717
31. Arioli M, Kruse C, Ruede U, Tardieu N. An iterative generalized Golub-Kahan algorithm for problems in structural mechanics. arXiv:1808.07677 [cs.CE]. 2018.

How to cite this article: Grubišić L, Tambača J. Direct solution method for the equilibrium problem for elastic stents. *Numer Linear Algebra Appl*. 2019;e2231. https://doi.org/10.1002/nla.2231